INTERNATIONAL JOURNAL FOR NUMERICAL METHODS IN FLUIDS, VOL. 13, 805–840 (1991)

LAGRANGIAN FINITE ELEMENT METHOD FOR FREE SURFACE NAVIER–STOKES FLOW USING FRACTIONAL STEP METHODS

MASAHIRO HAYASHI, KATSUMORI HATANAKA AND MUTSUTO KAWAHARA

Department of Civil Engineering, Chuo University, Kasuga, Bunkyo-ku, Tokyo, Japan

SUMMARY

This paper presents a finite element analysis based on the Lagrangian description for unsteady incompressible viscous fluid flow with a free surface. The behaviour of the fluid is expressed by the unsteady Navier–Stokes equation. For numerical integration in time the fractional step method is used. This method is useful because one can use the same linear interpolation functions for both velocity and pressure. In this paper, four variations of the fractional step method are presented and the numerical results are compared. To confirm the effectiveness of these methods, solitary wave propagation is analysed.

KEY WORDS Finite element method Lagrangian description Fractional step method Navier–Stokes equation Linear interpolation Free surface

1. INTRODUCTION

The analysis of unsteady incompressible viscous fluid flow with a free surface is of practical importance in the field of engineering. In this analysis, velocity and pressure should be determined considering the free surface. The position of the free surface is also unknown. Moreover, the boundary condition on the free surface is expressed by a complicated non-linear equation. Therefore the free surface flow is one of the most difficult problems to be solved by the numerical method. The problem is usually analysed on the basis of the Eulerian description, but it is rather inconvenient to express the complicated free surface configuration. Thus this paper uses the method based on the Lagrangian description. Employing the Lagrangian description, all finite elements in the analysis domain will move with the fluid. This fact considerably simplifies the treatment of the movement of the free surface boundary, which is varying in time.

The basic equation of the present method is the unsteady Navier–Stokes equation. For numerical integration in time the fractional step method is employed. In general, to solve the unsteady Navier–Stokes equation using the finite element method, the polynomial interpolation of velocity must be one order higher than that of pressure. This is usually called mixed interpolation. However, if mixed interpolation is used, the formulation itself, the computer programme and the preparation of the input data are quite complicated. In contrast to this, the linear interpolation function of the same order can be used for both velocity and pressure in the analysis of the fractional step method. Thus this method makes the computational scheme extremely simple.

The fractional step method is classified as one of the semi-implicit schemes. The unsteady Navier–Stokes equation can be transformed into a form in which velocity and pressure can be

0271–2091/91/170805–36$18.00

Received May 1990
Revised December 1990

computed in an independent manner, i.e. velocity is computed by the explicit scheme and pressure is obtained by the implicit scheme using the resultant velocity. For the interpolation function the three-node triangular element is employed for both velocity and pressure. The velocity correction method is one of the fractional step methods. The basic idea of this method was originally presented by Chorin[1] for the finite difference method. Donea *et al.*,[2,3] Schneider and co-workers,[4,5] Glowinsky *et al.*,[6] Mizukami and Tsuchiya[7] and Kawahara and Ohmiya[8] have adopted a similar approach to the Eulerian description of the Navier–Stokes equation in the case of the finite element method. In this paper the velocity correction method for the Lagrangian equation system is presented and is called Method A. Ramaswamy and co-workers[9,10] and Kawahara and Anjyu[11] have presented the Lagrangian finite element method. An improved method of this type, called Method B, is used in this paper. There are several problems with the boundary condition in these two methods. Thus two other methods, Methods C and D, are also presented in this paper. Method D employs the iteration based on Method C, but numerical experiments performed by the authors' group show that the numerical computation by Method C is more effective in practice. Moreover, Ramaswamy and Kawahara[12] have presented the arbitrary Lagrangian–Eulerian (ALE) finite element method. The ALE technique is suitable for the computation of highly non-linear problems, but this requires a large amount of computational time. Thus the Lagrangian method is more recommendable from the computational point of view. To validate these methods, solitary wave propagation has been analysed. Using the numerical experiments, the efficiency of the methods presented in this paper is discussed and compared.

2. BASIC EQUATIONS

Throughout this paper the equations are described using indicial notation and the summation convention for repeated indices. Two-dimensional unsteady incompressible viscous flow is dealt with, which is expressed by the unsteady Navier–Stokes equation. Let V be the fluid domain surrounded by a piecewise smooth boundary S.

The basic equations can be expressed using the fixed Cartesian co-ordinate system x_i shown in Figure 1. This co-ordinate system is usually referred to as the Eulerian co-ordinate system. The velocity and pressure fields are defined as functions of the spatial co-ordinate x_i:

$$u_i = u_i(x_i, t), \tag{1}$$

$$p = p(x_i, t). \tag{2}$$

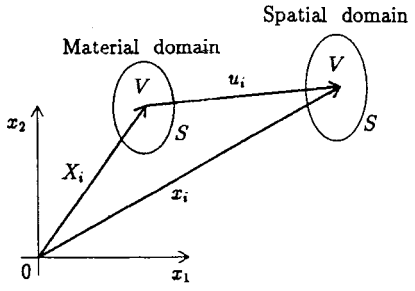

Figure 1. Co-ordinate system

The equation of motion can be written as

$$\left.\frac{Du_i}{Dt}\right|_{x_i}+\frac{1}{\rho}p_{,i}-\nu(u_{i,j}+u_{j,i})_{,j}=f_i \quad \text{in } V, \tag{3}$$

where ρ, ν and f_i denote fluid density, kinematic viscosity coefficient and body forces respectively. A subscript comma ',i' denotes differentiation with respect to co-ordinate x_i, while $(D/Dt)|_{x_i}$ means differentiation with respect to time t on the condition that co-ordinate x_i is fixed. The equation of continuity is

$$u_{i,i}=0 \quad \text{in } V. \tag{4}$$

The boundary S consists of two types of boundaries: one is the boundary S_1 on which velocity is given; the other is the boundary S_2 on which the surface force is specified. The boundary conditions for the basic equations can be expressed in the form

$$u_i=\hat{u}_i \quad \text{on } S_1, \tag{5}$$

$$\left(-\frac{1}{\rho}p\delta_{ij}+\nu(u_{i,j}+u_{j,i})\right)\cdot n_j=\hat{t}_i \quad \text{on } S_2, \tag{6}$$

where the superscript caret denotes a function which is given on the boundary, n_j means the direction cosine of the outward normal to the boundary with respect to co-ordinate x_j, and δ_{ij} is Kronecker's delta. The free surface condition is expressed as

$$\left.\frac{D\eta}{Dt}\right|_{x_i}=0 \quad \text{on } S_f, \tag{7}$$

where η is the position of the free surface and S_f means the free surface. As the initial condition, velocity and pressure are given over the whole flow field:

$$u_i=u_i^0(x_i), \tag{8}$$

$$p=p^0(x_i), \tag{9}$$

where u_i^0 and p^0 are velocity and pressure at time $t=0$ respectively.

The first term on the left-hand side of equation (3) represents the material differentiation. Introducing the material co-ordinate X_i, velocity and pressure concerned with the spatial co-ordinate x_i can be transformed into the form

$$U_i(X_i, t)=u_i(x_i, t), \tag{10}$$

$$P(X_i, t)=p(x_i, t). \tag{11}$$

The co-ordinate X_i is usually referred to as the Lagrangian co-ordinate. Using equations (10) and (11), equations (3)–(7) can be rewritten in the following form. The equations of motion and continuity are

$$\left.\frac{DU_i}{Dt}\right|_{X_i}+\frac{1}{\rho}P_{,i}-\nu(U_{i,j}+U_{j,i})_{,j}=F_i \quad \text{in } V, \tag{12}$$

$$U_{i,i}=0 \quad \text{in } V, \tag{13}$$

the boundary conditions on S_1 and S_2 are

$$U_i=\hat{U}_i \quad \text{on } S_1, \tag{14}$$

$$\left(-\frac{1}{\rho}P\delta_{ij}+\nu(U_{i,j}+U_{j,i})\right)\cdot N_j=\hat{T}_i \quad \text{on } S_2, \tag{15}$$

and the free surface condition is

$$\left.\frac{DY}{Dt}\right|_{X_i}=0 \quad \text{on } S_f, \tag{16}$$

where F_i and N_j are body forces and the direction cosine of the outward normal on the boundary in terms of the co-ordinate X_i respectively. The position of the free surface is

$$Y(X_i, t)=\eta(x_i, t), \tag{17}$$

where Y is the free surface position in terms of the co-ordinate X_i. As the initial condition, velocity and pressure are given as functions of the material co-ordinate X_i:

$$U_i=U_i^0(X_i), \tag{18}$$

$$P=P^0(X_i), \tag{19}$$

where U_i^0 and P^0 are velocity and pressure at time $t=0$ respectively.

3. NUMERICAL APPROXIMATIONS

The total time T is divided into a number of short time increments Δt. Each time point is denoted by n. Velocity and pressure at the nth time point can be defined as

$$U_i^n=U_i(X_i^n, t^n), \tag{20}$$

$$P^n=P(X_i^n, t^n), \tag{21}$$

where X_i^n denotes the Lagrangian co-ordinate at the nth time point. Velocity and pressure at the $(n+1)$th time point can be defined in the form

$$U_i^{n+1}=U_i(X_i^{n+1}, t^{n+1}), \tag{22}$$

$$P^{n+1}=P(X_i^{n+1}, t^{n+1}). \tag{23}$$

The Lagrangian co-ordinate X_i^{n+1} is expressed as

$$X_i^{n+1}\equiv x_i^{n+1}\simeq x_i^n+\frac{\Delta t}{2}(U_i^n+U_i^{n+1}). \tag{24}$$

From equation (16) the free surface position can be obtained as

$$Y(X_i^{n+1}, t^{n+1})=Y(X_i^{n+1}, t^n). \tag{25}$$

This means that the free surface position always takes the same value as a function of the Lagrangian co-ordinate X_i. Namely, this fact expresses that the fluid particle on the free surface always remains on the free surface. In a practical computation it is not necessary to take equation (25) into account. In the Lagrangian treatment, using equations (20) and (22), the material differentiation can be approximated in the form

$$\left.\frac{DU_i}{Dt}\right|_{X_i}\simeq\frac{U_i^{n+1}-U_i^n}{\Delta t}. \tag{26}$$

Substituting equation (26) into equation (12), the equation of motion can be discretized into

$$\frac{U_i^{n+1}-U_i^n}{\Delta t}=-\frac{1}{\rho}P_{,i}^{n+1}+\nu(U_{i,j}^n+U_{j,i}^n)_{,j}+F_i^n. \tag{27}$$

The equation of continuity is discretized as

$$U_{i,i}^{n+1}=0. \tag{28}$$

The boundary conditions corresponding to equations (14) and (15) are described by

$$U_i^{n+1}=\hat{U}_i \quad \text{on } S_1, \tag{29}$$

$$\left(-\frac{1}{\rho}P^{n+1}\delta_{ij}+\nu(U_{i,j}^{n+1}+U_{j,i}^{n+1})\right)\cdot N_j=\hat{T}_i \quad \text{on } S_2. \tag{30}$$

The analysis presented in this paper is to pursue the unknown variables U_i^{n+1} and P^{n+1} to satisfy equations (27) and (28) with the boundary conditions (29) and (30) starting from the known variables U_i^n and P^n.

For the discritization of the material function the finite element method is successfully used. The interpolations for velocity and pressure can be expressed as

$$U_i=\Phi_\alpha U_{\alpha i}, \tag{31}$$

$$P=\Phi_\alpha P_\alpha, \tag{32}$$

where Φ_α is the interpolation function and $U_{\alpha i}$ and P_α represent the nodal values at the αth node of the finite element. The corresponding weighting functions are expressed in the form

$$U_i^*=\Phi_\alpha U_{\alpha i}^*, \tag{33}$$

$$P^*=\Phi_\alpha P_\alpha^*. \tag{34}$$

The correction potential ϕ and the corresponding weighting function will be intoduced and interpolated as follows:

$$\phi=\Phi_\alpha\phi_\alpha, \tag{35}$$

$$\phi^*=\Phi_\alpha\phi_\alpha^*. \tag{36}$$

In the conventional analysis the mixed interpolation for velocity and pressure is usually used. In contrast, this paper employs equations (31)–(36) as the interpolation equations. This can be done because velocity and pressure can be computed employing the mutually independent equations. The linear interpolation function based on the three-node triangular element for both velocity and pressure is employed. The usual finite element procedure leads to the finite element equation. The precise form will be described in the following sections.

4. NUMERICAL STUDIES

For numerical studies the propagation and deformation of a solitary wave in a rectangular channel are calculated. If the stillwater depth is uniform, the solitary wave propagates without deformation. Referring to this phenomenon, the reliability of the analysis can be investigated. A solitary wave is essentially a wave that has infinite wavelength, but in this study the behaviour in a channel of limited length is examined. The splashing of the solitary wave is also investigated to the walls of both sides of the channel. The initial condition is assumed as Laitone's first approximation:[13]

$$C=\sqrt{\left[gd\left(1+\frac{H}{d}\right)\right]}, \tag{37}$$

$$U=\sqrt{(gd)}\left(\frac{H}{d}\right)\operatorname{sech}^2\left[\sqrt{\left(\frac{3}{4}\frac{H}{d^3}\right)}(X-Ct)\right], \tag{38}$$

$$V=\sqrt{(3gd)}\left(\frac{H}{d}\right)^{3/2}\left(\frac{Y}{d}\right)\operatorname{sech}^2\left[\sqrt{\left(\frac{3}{4}\frac{H}{d^3}\right)}(X-Ct)\right]\tanh\left[\sqrt{\left(\frac{3}{4}\frac{H}{d^3}\right)}(X-Ct)\right], \tag{39}$$

$$Y_s=d+H\operatorname{sech}^2\left[\sqrt{\left(\frac{3}{4}\frac{H}{d^3}\right)}(X-Ct)\right], \tag{40}$$

$$P=\rho g(Y_s-Y), \tag{41}$$

where C, U, V, P and Y_s denote wave velocity, velocities of directions X and Y, pressure and wave height from the bottom respectively and g, d and H represent gravitational acceleration, water depth and wave height of a solitary wave respectively. To examine the run-up height R of a solitary wave on a vertical wall, an analytical approximation can be obtained by the following equation:

$$R=2d\left(\frac{H}{d}\right)+\frac{d}{2}\left(\frac{H}{d}\right)^2. \tag{42}$$

To decide the channel length L, the following equation is used:

$$\frac{L}{d}\geqslant 6{\cdot}9\left(\frac{d}{H}\right)^{1/2} \tag{43}$$

The analysis domain is limited to the place where the wave height of the solitary wave is equal to or less than $H/1000$. This value is determined considering the length of the analysis domain to be effective for the solitary wave. Thus equation (42) is obtained by Laitone's approximation (Figure 2).

As numerical studies, two types of solitary wave are analysed. The dimensions and conditions of the wave of Example 1 are given in Tables I and II. The initial condition is shown in Figure 3. In this figure the scale of direction Y is 10 times larger than that of direction X. The figure shows the finite element mesh, velocity vectors and pressure distribution. Example 2 is a wave which is higher than that of Example 1. The dimensions and conditions of Example 2 are shown in Tables II and III. The initial condition is shown in Figure 4. The scale of direction Y is four times larger than that of direction X.

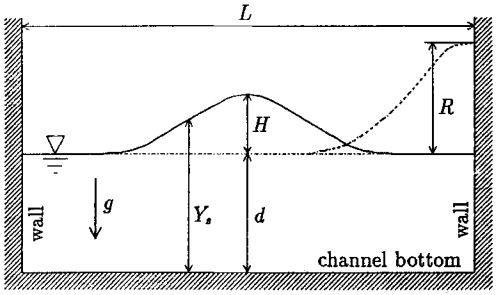

Figure 2. Solitary wave profile

Initial condition

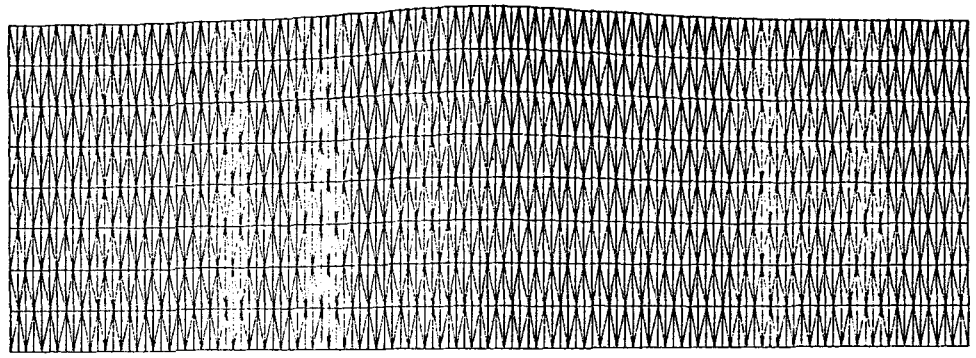

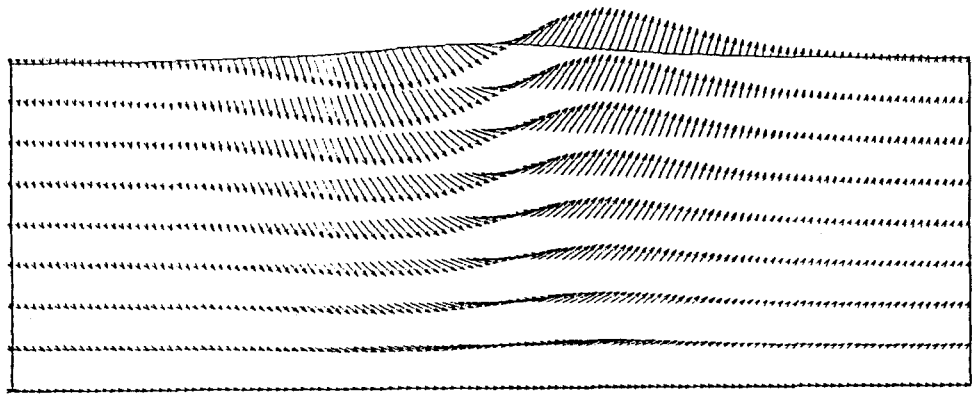

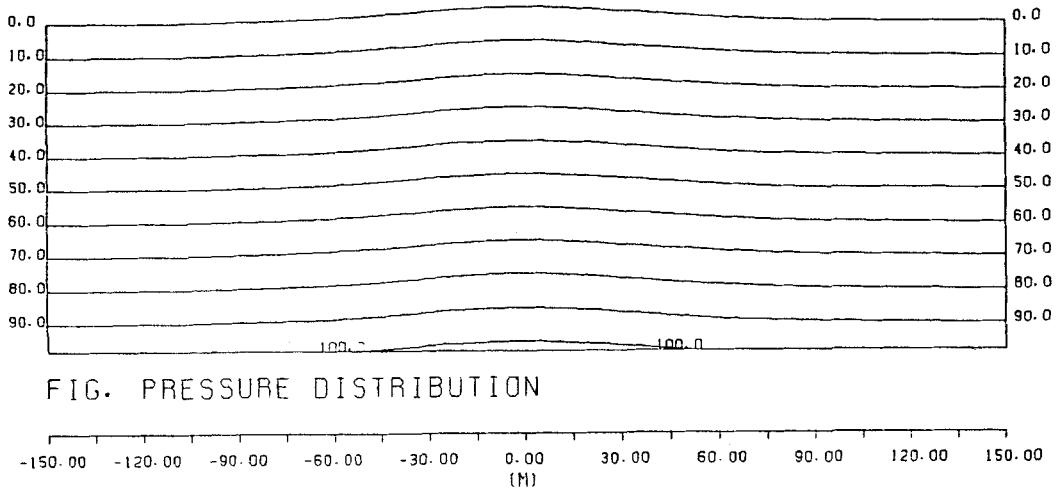

Figure 3. Initial condition of Example 1

Table I. Solitary wave Example I

Length of channel	300 m
Stillwater depth	10 m
Wave height	0·5 m
Total number of nodal points	1089
Total number of elements	1920
ΔX	2·5 m
ΔY	1·25 m

Table II. Computational conditions of Examples 1 and 2

Time increment	0·01 s
Density	1 t m^{-3}
Kinematic viscosity coefficient	0 m^2 s^{-1}
Gravitational acceleration	9·8 m s^{-2}

Table III. Solitary wave Example 2

Length of channel	160 m
Still water depth	10 m
Wave height	2 m
Total number of nodal points	1161
Total number of elements	2048
ΔX	1·25 m
ΔY	1·25 m

5. METHOD A

5.1. *Basic concept*

The numerical analysis referred to as Method A (the velocity correction method) is described in this section. By discretizing the equation of motion, the intermediate velocity can be obtained. However, this velocity may not satisfy the equation of continuity. To correct the obtained intermediate velocity, the correction potential is introduced. Using the equation of continuity, the Poisson equation can be derived for the correction potential. To solve the resultant Poisson equation, the correction velocity can be derived.

Referring to equation (27), the intermediate velocity $\tilde{U}_i^{n+1}$ is defined in the form

$$\frac{\tilde{U}_i^{n+1}-U_i^n}{\Delta t}=-\frac{1}{\rho}P_{,i}^n+\nu(U_{i,j}^n+U_{j,i}^n)_{,j}+F_i^n. \tag{44}$$

The intermediate velocity $\tilde{U}_i^{n+1}$ may not satisfy the equation of continuity. Thus velocity U_i^{n+1} can be obtained by correcting the intermediate velocity $\tilde{U}_i^{n+1}$ to satisfy the equation of continuity. Taking the rotation on both sides of equations (27) and (44), the following relation can be obtained:

$$\text{rot}\, U_i^{n+1}=\text{rot}\, \tilde{U}_i^{n+1}. \tag{45}$$

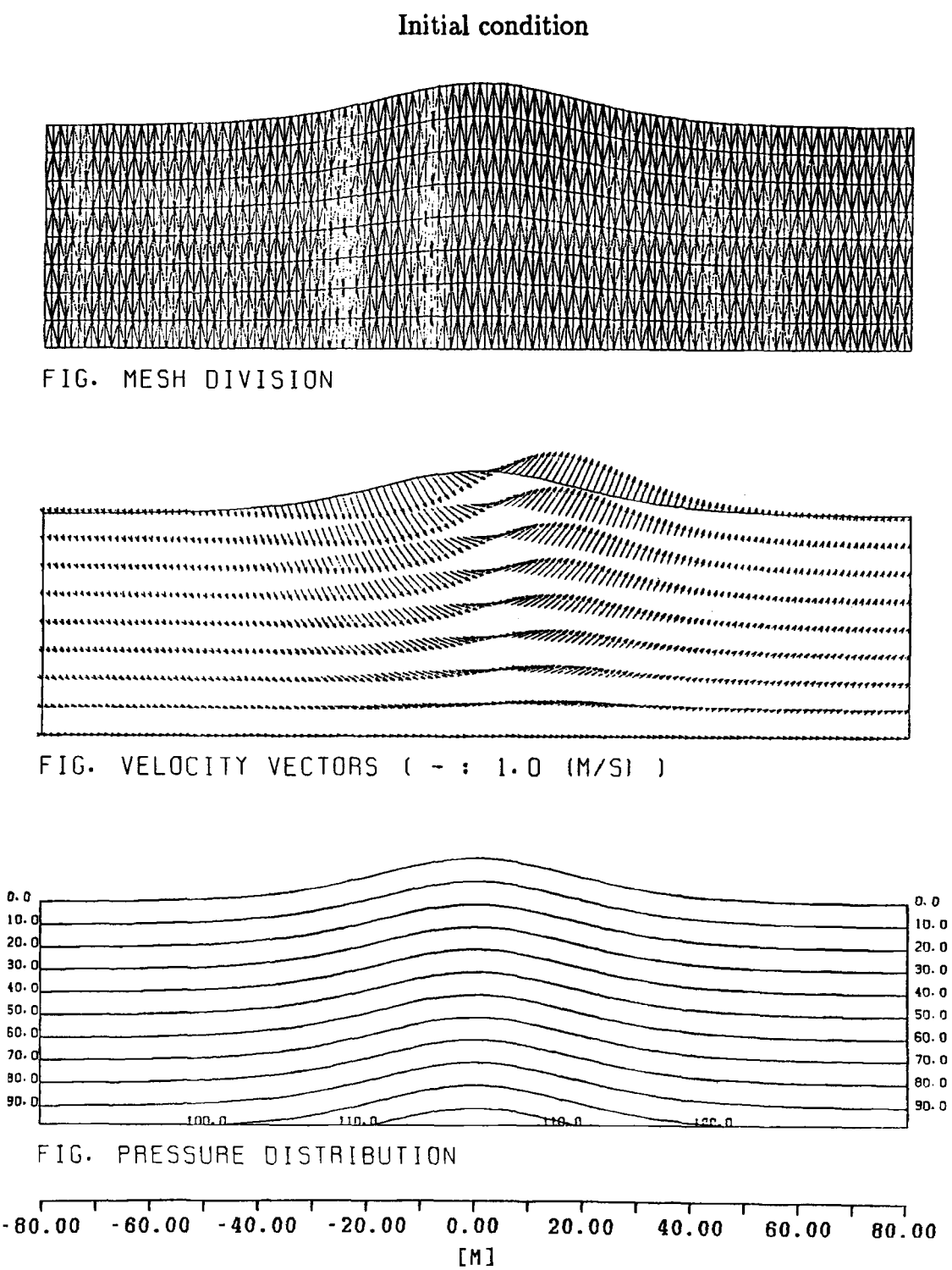

Figure 4. Initial condition of Example 2

This equation means that

$$U_i^{n+1} = \tilde{U}_i^{n+1} + \phi_{,i}, \tag{46}$$

where ϕ is a scalar which is referred to as the correction potential. Taking the divergence on both sides of equation (46), it follows that

$$U_{i,i}^{n+1} = \tilde{U}_{i,i}^{n+1} + \phi_{,ii}, \tag{47}$$

Substituting the equation of continuity (28) into equation (47), the equation for ϕ can be derived as

$$\phi_{,ii} = -\tilde{U}_{i,i}^{n+1}. \tag{48}$$

Substituting equations (27) and (44) into equation (47), the equation of pressure can be expressed as

$$P_{,i}^{n+1} = P_{,i}^{n} - \frac{\rho}{\Delta t}\phi_{,i}. \tag{49}$$

Integrating equation (49) and defining the integral constant as zero, the equation for pressure is described in the form

$$P^{n+1} = P^n - \frac{\rho}{\Delta t}\phi. \tag{50}$$

The algorithm of Method A can be summarized as follows.

1. The intermediate velocity $\tilde{U}_i^{n+1}$ is calculated:

$$\tilde{U}_i^{n+1} = U_i^n - \Delta t\left(\frac{1}{\rho}P_{,i}^n - \nu(U_{i,j}^n + U_{j,i}^n)_{,j} - F_i^n\right). \tag{51}$$

2. Correction potential ϕ is calculated:

$$\phi_{,ii} = -\tilde{U}_{i,i}^{n+1}. \tag{52}$$

3. Velocity U_i^{n+1} is calculated:

$$U_i^{n+1} = \tilde{U}_i^{n+1} + \phi_{,i}. \tag{53}$$

4. Pressure P^{n+1} is calculated:

$$P^{n+1} = P^n - \frac{\rho}{\Delta t}\phi. \tag{54}$$

5. U_i^{n+1}, P^{n+1} are replaced with U_i^{n+1}, P^n and proceed to the next time cycle.

5.2. Variational equations

To obtain the finite element equations, the variational forms should be derived. Equation (51) is multiplied by the weighting function U_i^* and integrated by parts over the domain V to give

$$\int_V (U_i^* \tilde{U}_i^{n+1})\mathrm{d}V = \int_V (U_i^* U_i^n)\mathrm{d}V + \Delta t\left(\frac{1}{\rho}\int_V (U_{i,i}^* P^n)\mathrm{d}V - \nu\int_V U_{i,j}^*(U_{i,j}^n + U_{j,i}^n)\mathrm{d}V + \int_V (U_i^* F_i^n)\mathrm{d}V + \Sigma_i^n\right), \tag{55}$$

$$\Sigma_i^n = \int_S U_i^* \left(-\frac{1}{\rho} P^n \cdot \delta_{ij} + \nu (U_{i,j}^n + U_{j,i}^n) \right) \cdot N_j \, \mathrm{d}S. \tag{56}$$

Equation (52) is multiplied by the weighting function ϕ^* and integrated by parts over the domain V to give

$$\int_V (\phi_{,i}^* \phi_{,i}) \mathrm{d}V = \int_V (\phi^* \tilde{U}_{i,i}^{n+1}) \mathrm{d}V + \int_S (\phi^* \phi_{,i}) \cdot N_i \mathrm{d}S. \tag{57}$$

Equation (53) is multiplied by the weighting function U_i^* and integrated by parts over the domain V to give

$$\int_V (U_i^* U_i^{n+1}) \mathrm{d}V = \int_V (U_i^* \tilde{U}_i^{n+1}) \mathrm{d}V + \int_V (U_i^* \phi_{,i}) \mathrm{d}V. \tag{58}$$

Equation (54) is multiplied by the weighting function P^* and integrated by parts over the domain V to give

$$\int_V (P^* P^{n+1}) \mathrm{d}V = \int_V (P^* P^n) \mathrm{d}V - \frac{\rho}{\Delta t} \int_V (P^* \phi) \mathrm{d}V. \tag{59}$$

On the basis of equations (55)–(59) the finite element method will be derived. As the natural boundary conditions, several types of boundary conditions are included in the variational equations. Therefore it is necessary to clarify the natural boundary conditions which can be handled with these variational equations before the finite element equations are formulated.

5.3. *Boundary conditions*

The boundary conditions in Figure 5 can be explained as follows:

(i)
$$\tilde{U}_i^{n+1} = \hat{U}_i \qquad \text{on } S_1, \tag{60}$$

$$\left(-\frac{1}{\rho} P^n \cdot \delta_{ij} + \nu (U_{i,j}^n + U_{j,i}^n) \right) \cdot N_j = \hat{t}_i = 0 \qquad \text{on } S_2; \tag{61}$$

(ii)
$$\phi_{,i} \cdot N_i = \hat{r}_i \qquad \text{on } S_1, \tag{62}$$

$$\phi = \hat{\phi} \qquad \text{on } S_2; \tag{63}$$

(iii)
$$U_i^{n+1} = \hat{U}_i \qquad \text{on } S_1. \tag{64}$$

Item (i) is the boundary condition associated with equation (51). Equation (60) means that the intermediate velocity on the boundary is assumed to be the same as the boundary velocity.

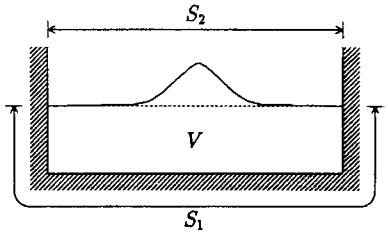

Figure 5. Boundary condition

Equation (61) expresses the fact that the surface force is zero on the free surface boundary. Equation (61) can be considered as the natural boundary condition of equation (56). Item (ii) is associated with equation (52). The boundary condition expressed by equation (62) can be imposed as the natural boundary condition of equation (57). Normally $\hat{t}_i$ is given as zero. This means that the normal gradient of pressure must always be constant with respect to time. Equation (63) gives the fundamental basis on which the pressure is measured. Thus normally function $\hat{\phi}$ is given as zero. Item (iii) is the boundary condition for the new velocity computed at the $(n+1)$th time point.

5.4. *Finite element equations*

The finite element equations can be derived in the following form from equations (55) and (57)–(59) using the interpolation function equations (31), (32) and (35) and the weighting function equations (33), (34) and (36):

$$\bar{M}^{n+1}_{\alpha\beta}\tilde{U}^{n+1}_{\beta i}=\bar{M}^{n}_{\alpha\beta}U^{n}_{\beta i}+\Delta t\left(\frac{1}{\rho}H^{n}_{\alpha i\beta}P^{n}_{\beta}-\nu S^{n}_{\alpha i\beta j}U^{n}_{\beta j}+N^{n}_{\alpha}F^{n}_{\alpha i}+\hat{\Sigma}^{n}_{\alpha i}\right), \tag{65}$$

$$A^{n+1}_{\alpha i\beta i}\phi_{\beta}=H^{n+1}_{\alpha\beta i}\tilde{U}^{n+1}_{\beta i}+\hat{\Omega}^{n+1}_{\alpha i}, \tag{66}$$

$$\bar{M}^{n+1}_{\alpha\beta}U^{n+1}_{\beta i}=\bar{M}^{n+1}_{\alpha\beta}\tilde{U}^{n+1}_{\beta i}+H^{n+1}_{\alpha\beta i}\phi_{\beta}, \tag{67}$$

$$\bar{M}^{n+1}_{\alpha\beta}P^{n+1}_{\beta}=\bar{M}^{n}_{\alpha\beta}P^{n}_{\beta}-\frac{\rho}{\Delta t}\bar{M}^{n+1}_{\alpha\beta}\phi_{\beta}, \tag{68}$$

where

$$M_{\alpha\beta}=\int_V(\Phi_{\alpha}\Phi)\mathrm{d}V, \qquad N_{\alpha}=\int_V(\Phi_{\alpha})\mathrm{d}V,$$

$$S_{\alpha i\beta j}=\int_V(\Phi_{\alpha,k}\Phi_{\beta,k})\mathrm{d}V\cdot\delta_{ij}+\int_V(\Phi_{\alpha,j}\Phi_{\beta,i})\mathrm{d}V,$$

$$A_{\alpha i\beta i}=\int_V(\Phi_{\alpha,i}\Phi_{\beta,i})\mathrm{d}V, \qquad H_{\alpha\beta i}=\int_V(\Phi_{\alpha}\Phi_{\beta,i})\mathrm{d}V, \qquad H_{\alpha i\beta}=H^{T}_{\alpha i},$$

$$\hat{\Omega}_{\alpha i}=\int_S(\Phi_{\alpha}\hat{t}_i)\mathrm{d}S, \qquad \hat{\Sigma}_{\alpha i}=\int_S(\Phi_{\alpha}\hat{t}_i)\mathrm{d}S,$$

in which $\bar{M}_{\alpha\beta}$ means the lumped mass matrix obtained from the consistent matrix $\mathbf{M}_{\alpha\beta}$. Superscript n expresses the value at the nth time point. Superscript n of the matrix denotes the time point at which the coefficient matrix is computed. Using the Lagrangian finite element method, the element form changes at each time point, because the domain to be analysed changes in time. Thus the coefficient matrix should be reformulated at each time point. The co-ordinate at the $(n+1)$th time point is originally unknown but can be calculated using iteration.

5.5. *Algorithm*

The algorithm of the Lagrangian finite element method using Method A can be expressed in the following form

(a) Set $m=0$ and $U^{n+1(0)}_i$ is assigned as U^n_i.
(b) The co-ordinates of the nodal points $X^{n+1(m)}_i$ are calculated:

$$X^{n+1(m)}_i=X^n_i+\frac{\Delta t}{2}(U^{n+1(m)}_i+U^n_i). \tag{69}$$

(c) The intermediate velocity $\tilde{U}_i^{n+1}$ is calculated:

$$\bar{M}_{\alpha\beta}^{n+1}\tilde{U}_{\beta i}^{n+1}=\bar{M}_{\alpha\beta}^{n}U_{\beta i}^{n}+\Delta t\left(\frac{1}{\rho}H_{\alpha i\beta}^{n}P_{\beta}^{n}-\nu S_{\alpha i\beta j}^{n}U_{\beta j}^{n}+N_{\alpha}^{n}F_{\alpha i}^{n}+\hat{\Sigma}_{\alpha i}^{n}\right). \tag{70}$$

(d) Correction potential ϕ is calculated:

$$A_{\alpha i\beta i}^{n+1}\phi_{\beta}=H_{\alpha\beta i}^{n+1}\tilde{U}_{\beta i}^{n+1}+\hat{\Omega}_{\alpha i}^{n+1}. \tag{71}$$

(e) Velocity $U_i^{n+1(m+1)}$ is calculated:

$$\bar{M}_{\alpha\beta}^{n+1}U_{\beta i}^{n+1(m+1)}=\bar{M}_{\alpha\beta}^{n+1}\tilde{U}_{\beta i}^{n+1}+H_{\alpha\beta i}^{n+1}\phi_{\beta}. \tag{72}$$

(f) Pressure $P^{n+1(m+1)}$ is calculated:

$$\bar{M}_{\alpha\beta}^{n+1}P_{\beta}^{n+1(m+1)}=\bar{M}_{\alpha\beta}^{n}P_{\beta}^{n}-\frac{\rho}{\Delta t}\bar{M}_{\alpha\beta}^{n+1}\phi_{\beta}. \tag{73}$$

(g) If $|U_i^{n+1(m+1)}-U_i^{n+1(m)}|<\varepsilon$ is not satisfied, then $m=m+1$ and return to step (b).

(h) $U_i^{n+1(m+1)}$, $P^{n+1(m+1)}$ are replaced with U_i^n, P^n and proceed to the next iteration cycle.

The number of iterations within one time point is denoted by (m).

5.6. *Numerical study*

Figure 6 shows the finite element mesh representing the solitary wave propagation, the computed velocity and pressure at the times when the run-up height of a solitary wave on a right wall becomes maximum, when the wave returns to the centred position, when the run-up height of a solitary wave on a left wall becomes maximum and when the wave returns to the centred position again. The final computed results should be coincident with the initial configuration because the viscosity is neglected in this computation. Identical results have been obtained, which shows that the algorithm of Method A is adaptable to the analysis of free surface flows such as solitary wave propagation.

6. METHOD B

6.1. *Basic concept*

The numerical analysis referred to as Method B (the velocity correction method) is described in this section. Let separate the discretized equation of motion into two parts, the terms of velocity and pressure. The quantity which can be computed by the equation of motion dropping the pressure term is referred to as the intermediate velocity in this section. The intermediate velocity would not satisfy the equation of continuity. Therefore the pressure equation can be derived so as to satisfy the equation of continuity.

The equation of motion can be split into two terms as

$$U_i^{n+1}=\tilde{U}_i^{n+1}+\Delta U_i, \tag{74}$$

where $\tilde{U}_i^{n+1}$ is referred to as the intermediate velocity and is defined in the form

$$\tilde{U}_i^{n+1}=U_i^n+\Delta t[\nu(U_{i,j}^n+U_{j,i}^n)_{,j}+F_i^n]. \tag{75}$$

The physical meaning of the intermediate velocity is not clear. The correction velocity ΔU_i can be determined by the pressure term as

$$\Delta U_i=U_i^{n+1}-\tilde{U}_i^{n+1}=-\frac{\Delta t}{\rho}P_{,i}^{n+1}. \tag{76}$$

step = 1491 , time = 14.91 (sec)

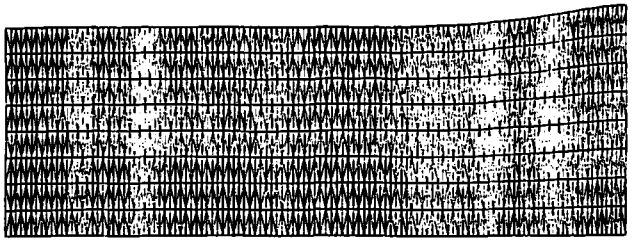

FIG. MESH DIVISION

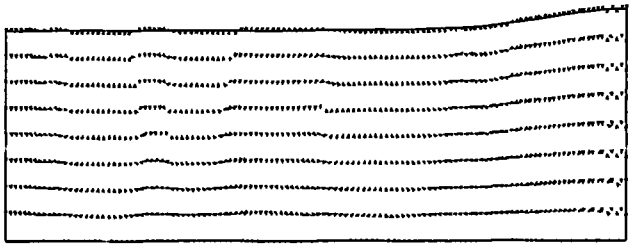

FIG. VELOCITY VECTORS (—— : 1.0 (M/S))

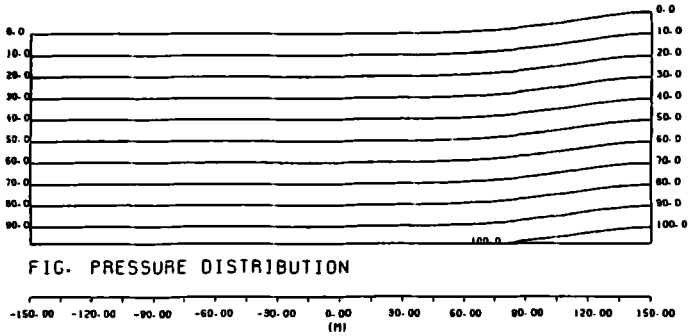

FIG. PRESSURE DISTRIBUTION

The run-up height on a right wall becomes maximum

step = 2982 , time = 29.82 (sec)

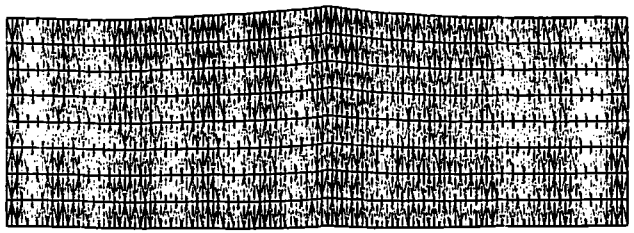

FIG. MESH DIVISION

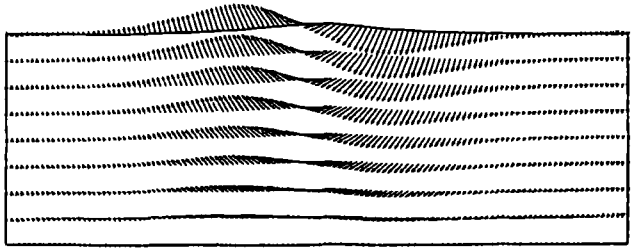

FIG. VELOCITY VECTORS (—— : 1.0 (M/S))

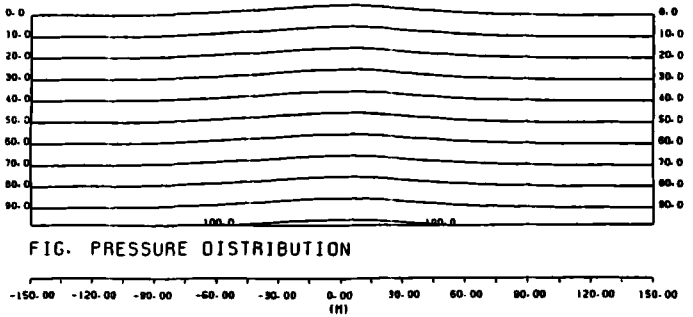

FIG. PRESSURE DISTRIBUTION

The wave returns to the center position

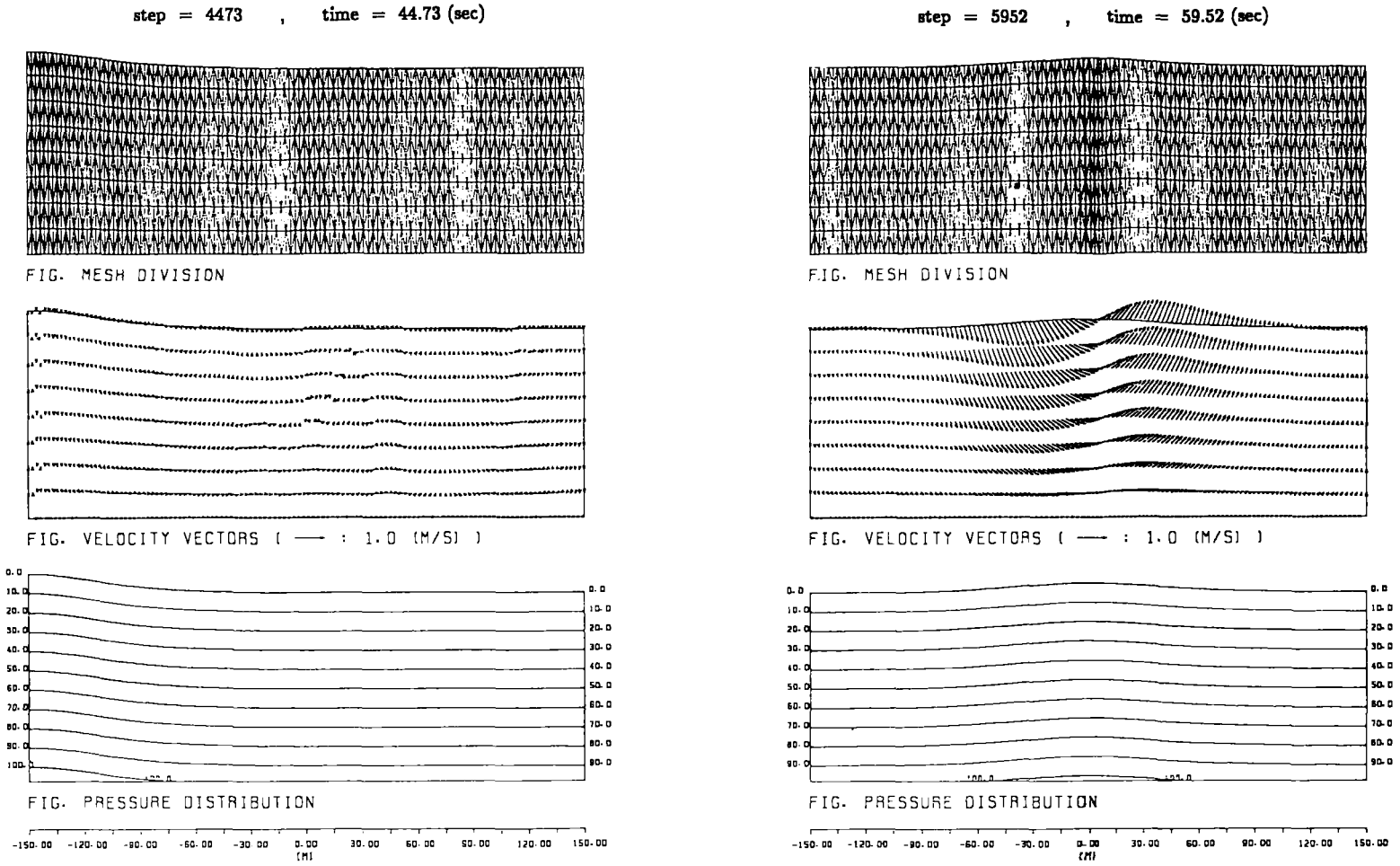

The run-up height on a left wall becomes maximum

The wave returns to the center position

Figure 6. Computed result by Method A

Thus equation (74) can be rewritten as

$$U_i^{n+1} = \tilde{U}_i^{n+1} - \frac{\Delta t}{\rho} P_{,i}^{n+1}. \tag{77}$$

Taking the divergence on both sides of equation (77) and substituting that equation into the equation of continuity (28), the pressure Poisson equation can be obtained as

$$P_{,ii}^{n+1} = \frac{\rho}{\Delta t} \tilde{U}_{i,i}^{n+1}. \tag{78}$$

The algorithm of Method B can be summarized as follows.

1. The intermediate velocity $\tilde{U}_i^{n+1}$ is calculated:

$$\tilde{U}_i^{n+1} = U_i^n + \Delta t[\nu(U_{i,j}^n + U_{j,i}^n)_{,j} + F_i^n]. \tag{79}$$

2. Pressure P^{n+1} is calculated:

$$P_{,ii}^{n+1} = \frac{\rho}{\Delta t} \tilde{U}_{i,i}^{n+1}. \tag{80}$$

3. Velocity U_i^{n+1} is calculated:

$$U_i^{n+1} = \tilde{U}_i^{n+1} - \frac{\Delta t}{\rho} P_{,i}^{n+1}. \tag{81}$$

4. U_i^{n+1} is replaced with U_i^n and proceed to the next time cycle.

6.2. *Variational equations*

To obtain the finite element equations, the variational forms should be derived. Equation (79) is multiplied by the weighting function U_i^* and integrated by parts over the domain V to give

$$\int_V (U_i^* \tilde{U}_i^{n+1}) \mathrm{d}V = \int_V (U_i^* U_i^n) \mathrm{d}V - \Delta t \left(\nu \int_V U_{i,j}^* (U_{i,j}^n + U_{j,i}^n) \mathrm{d}V - \int_V (U_i^* F_i^n) \mathrm{d}V - \Sigma_i^n \right), \tag{82}$$

$$\Sigma_i^n = \int_S U_i^* [\nu(U_{i,j}^n + U_{j,i}^n)] \cdot N_j \, \mathrm{d}S. \tag{83}$$

Equation (80) is multiplied by the weighting function P^* and integrated over the domain V to give

$$\int_V (P_{,i}^* P_{,i}^{n+1}) \mathrm{d}V = -\frac{\rho}{\Delta t} \int_V (P^* \tilde{U}_{i,i}^{n+1}) \, \mathrm{d}V + \int_S (P^* P_{,i}^{n+1}) \cdot N_i \, \mathrm{d}S. \tag{84}$$

Equation (81) is multiplied by the weighting function U_i^* and integrated by parts over the domain V to give

$$\int_V (U_i^* U_i^{n+1}) \, \mathrm{d}V = \int_V (U_i^* \tilde{U}_i^{n+1}) \, \mathrm{d}V - \frac{\Delta t}{\rho} \int_V (U_i^* P_{,i}^{n+1}) \mathrm{d}V. \tag{85}$$

On the basis of equations (82)–(85) the finite element method will be derived. As the natural boundary conditions, several conditions can be considered in the variational equations. Therefore it is necessary to clarify the natural boundary conditions which can be handled with these variational equations before the finite element equations are formulated.

6.3. Boundary conditions

The boundary conditions in Figure 7 can be explained as follows:

(i) $$[\nu(U^n_{i,j}+U^n_{j,i})]\cdot N_j=\hat{t}_i=0 \quad \text{on } S_2; \tag{86}$$

(ii) $$P^{n+1}_{,i}\cdot N_i=\hat{r}_i \quad \text{on } S_1, \tag{87}$$

$$P^{n+1}=\hat{P} \quad \text{on } S_2; \tag{88}$$

(iii) $$U^{n+1}_i=\hat{U}_i \quad \text{on } S_1. \tag{89}$$

Item (i) is the boundary condition associated with equation (79). It is important that no part of the intermediate velocity should be specified, because the intermediate velocity is not the actual velocity. If the boundary condition for the specified velocity was imposed on equation (79), the computation would be divergent. Equation (79) is the explicit form; therefore the computation can be carried out without any specified intermediate velocity boundary condition. Equation (86) corresponds to the free surface boundary condition with equation (88). Equation (87) should be discussed more precisely. The following four cases were carried out in our numerical experiments. For each boundary S_{1-1} and S_{1-2} shown in Figure 7 the boundary condition must be imposed separately:

⟨1⟩ $$\frac{\partial P^{n+1}}{\partial n}=\frac{\partial P^{n+1}}{\partial \tau}=0 \quad \text{on } S_{1-1}, S_{1-2}; \tag{90}$$

⟨2⟩ $$\frac{\partial P^{n+1}}{\partial n}=0 \quad \text{and} \quad \frac{\partial P^{n+1}}{\partial \tau}=\hat{r}_1 \quad (\hat{r}_1\neq 0) \quad \text{on } S_{1-1}, \tag{91}$$

$$\frac{\partial P^{n+1}}{\partial n}=\hat{r}_2 \quad (\hat{r}_2\neq 0) \quad \text{and} \quad \frac{\partial P^{n+1}}{\partial \tau}=0 \quad \text{on } S_{1-2}; \tag{92}$$

⟨3⟩ $$P^{n+1}=\hat{P}=\rho g h \quad \text{on } S_{1-1}, S_{1-2}; \tag{93}$$

⟨4⟩ $$\frac{\partial P^{n+1}}{\partial n}=0 \quad \text{and} \quad \frac{\partial P^{n+1}}{\partial \tau}=\rho g \quad \text{on } S_{1-1}, \tag{94}$$

$$\frac{\partial P^{n+1}}{\partial n}=\rho g \quad \text{and} \quad \frac{\partial P^{n+1}}{\partial \tau}=0 \quad \text{on } S_{1-2}. \tag{95}$$

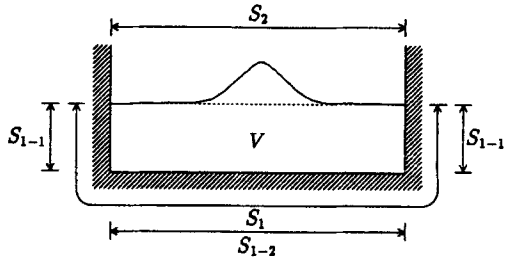

Figure 7. Boundary condition

Case ⟨1⟩ means that the pressure gradients both normal and tangential to the wall are equal to zero. Case ⟨2⟩ expresses that the pressure gradient in the normal direction on the boundary S_{1-1} and in the tangential direction on the boundary S_{1-2} are equal to zero. The two equations for r_1 and r_2 can be derived as follows. Separating the equation of motion into normal and tangential directions, we obtain

$$\frac{\partial P}{\partial n}=-\rho\left(\frac{\partial U_n}{\partial t}-\nu(U_{n,j}+U_{j,n}),_j-F_n\right), \tag{96}$$

$$\frac{\partial P}{\partial \tau}=-\rho\left(\frac{\partial U_\tau}{\partial t}-\nu(U_{\tau,j}+U_{j,\tau}),_j-F_\tau\right), \tag{97}$$

where it is found that the second and third terms of the right-hand sides are the parts of the intermediate velocity:

$$\nu(U^n_{i,j}+U^n_{j,i}),_j+F^n_i=\frac{\tilde{U}^{n+1}_i-U^n_i}{\Delta t}. \tag{98}$$

Using the intermediate velocity, the following expressions can be obtained:

$$r_1=\frac{\partial P^{n+1}}{\partial \tau}=-\rho\left(\frac{U^{n+1}_\tau-U^n_\tau}{\Delta t}-\frac{\tilde{U}^{n+1}_\tau-U^n_\tau}{\Delta t}\right)=\rho\frac{\tilde{U}^{n+1}_\tau-U^{n+1}_\tau}{\Delta t}, \tag{99}$$

$$r_2=\frac{\partial P^{n+1}}{\partial n}=-\rho\left(\frac{U^{n+1}_n-U^n_n}{\Delta t}-\frac{\tilde{U}^{n+1}_n-U^n_n}{\Delta t}\right)=\rho\frac{\tilde{U}^{n+1}_n-U^{n+1}_n}{\Delta t}. \tag{100}$$

In equations (99) and (100), putting $r_1=r_2=0$, the boundary conditions can be converted to those of the intermediate velocity:

$$\tilde{U}^{n+1}_\tau=\hat{U}^{n+1}_\tau, \tag{101}$$

$$\tilde{U}^{n+1}_n=\hat{U}^{n+1}_n. \tag{102}$$

Case ⟨3⟩ is the Dirichlet condition that pressure is specified on the boundaries S_{1-1} and S_{1-2}. Case ⟨4⟩ expresses that the pressure gradients tangential to the boundary S_{1-1} and normal to the boundary S_{1-2} are given. The free surface problem is analysed using these four cases of the boundary conditions. In computations by the authors' group, numerical results have been obtained only using the condition in case ⟨4⟩ for solitary wave propagation. This problem is the vertical two-dimensional problem including the gravitational effect. Thus the condition in case ⟨4⟩ seems useful. However, in the case of cavity flow the condition in case ⟨2⟩ would be useful.

6.4. *Finite element equations*

The finite element equations can be derived in the following form from equations (82), (84) and (85) using the interpolation function equations (31) and (32) and the weighting function equations (33) and (34):

$$\bar{M}^{n+1}_{\alpha\beta}\tilde{U}^{n+1}_{\beta i}=\bar{M}^n_{\alpha\beta}U^n_{\beta i}-\Delta t(\nu S^n_{\alpha i\beta i}U^n_{\beta j}-N^n_\alpha F^n_{\alpha i}-\hat{\Sigma}^n_{\alpha i}), \tag{103}$$

$$A^{n+1}_{\alpha i\beta i}P^{n+1}_\beta=-\frac{\rho}{\Delta t}H^{n+1}_{\alpha\beta i}\tilde{U}^{n+1}_{\beta i}+\hat{\Omega}^{n+1}_{\alpha i}, \tag{104}$$

$$\bar{M}^{n+1}_{\alpha\beta}U^{n+1}_{\beta i}=\bar{M}^{n+1}_{\alpha\beta}\tilde{U}^{n+1}_{\beta i}-\frac{\Delta t}{\rho}H^{n+1}_{\alpha\beta i}P^{n+1}_\beta, \tag{105}$$

where

$$M_{\alpha\beta}=\int_V(\Phi_\alpha\Phi_\beta)\mathrm{d}V, \qquad N_\alpha=\int_V(\Phi_\alpha)\mathrm{d}V,$$

$$S_{\alpha i\beta i}=\int_V(\Phi_{\alpha,k}\Phi_{\beta,k})\mathrm{d}V\cdot\delta_{ij}+\int_V(\Phi_{\alpha,j}\Phi_{\beta,i})\mathrm{d}V,$$

$$A_{\alpha i\beta i}=\int_V(\Phi_{\alpha,i}\Phi_{\beta,i})\mathrm{d}V, \quad H_{\alpha\beta i}=\int_V(\Phi_\alpha\Phi_{\beta,i})\mathrm{d}V,$$

$$\hat{\Omega}_{\alpha i}=\int_S(\Phi_\alpha\hat{r}_i)\mathrm{d}S, \qquad \hat{\Sigma}_{\alpha i}=\int_S(\Phi_\alpha\hat{t}_i)\mathrm{d}S,$$

in which $\bar{M}_{\alpha\beta}$ means the lumped mass matrix obtained from the consistent matrix $M_{\alpha\beta}$.

6.5. *Algorithm*

The algorithm of the Lagrangian finite element method using Method B can be expressed in the following form.

(a) Set $m=0$ and $U_i^{n+1(0)}$ is assigned as U_i^n.
(b) The co-ordinates of the nodal points $X_i^{n+1(m)}$ are calculated:

$$X_i^{n+1(m)}=X_i^n+\frac{\Delta t}{2}(U_i^{n+1(m)}+U_i^n). \tag{106}$$

(c) The intermediate velocity $\tilde{U}_i^{n+1}$ is calculated:

$$\bar{M}_{\alpha\beta}^{n+1}\tilde{U}_{\beta i}^{n+1}=\bar{M}_{\alpha\beta}^{n}U_{\beta i}^{n}-\Delta t(\nu S_{\alpha i\beta i}^{n}U_{\beta j}^{n}-N_\alpha^n F_{\alpha i}^n-\hat{\Sigma}_{\alpha i}^n). \tag{107}$$

(d) Pressure $P^{n+1(m+1)}$ is calculated:

$$A_{\alpha i\beta i}^{n+1}P_\beta^{n+1(m+1)}=-\frac{\rho}{\Delta t}H_{\alpha\beta i}^{n+1}\tilde{U}_{\beta i}^{n+1}+\hat{\Omega}_{\alpha i}^{n+1}. \tag{108}$$

(e) Velocity $U_i^{n+1(m+1)}$ is calculated:

$$\bar{M}_{\alpha\beta}^{n+1}U_{\beta i}^{n+1(m+1)}=\bar{M}_{\alpha\beta}^{n+1}\tilde{U}_{\beta i}^{n+1}-\frac{\Delta t}{\rho}H_{\alpha\beta i}^{n+1}P_\beta^{n+1(m+1)}. \tag{109}$$

(f) If $|U_i^{n+1(m+1)}-U_i^{n+1(m)}|<\varepsilon$ is not satisfied, then $m=m+1$ and return to step (b).
(g) $U_i^{n+1(m+1)}$ is replaced with U_i^n, and proceed to the next iteration cycle.

The number of iterations within one time point is denoted by (m).

6.6. *Numerical study*

Figure 8 shows the finite element mesh representing the solitary wave propagation, the computed velocity and pressure at the times when the run-up height of a solitary wave on a right wall becomes maximum, when the wave returns to the centred position, when the run-up height of a solitary wave on a left wall becomes maximum and when the wave returns to the centred position again. The final computed results should be coincident with the initial configuration because the viscosity is neglected in this computation. Identical results have been obtained, which shows that the algorithm of Method B is adaptable to the analysis of free surface flows such as solitary wave propagation.

step = 1491 , time = 14.91 (sec)

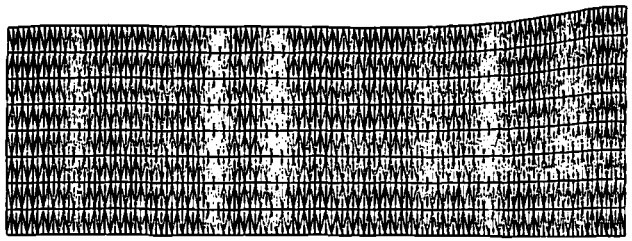

FIG. MESH DIVISION

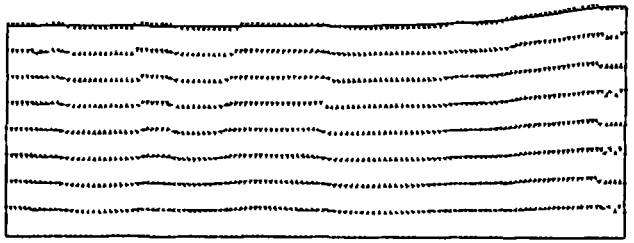

FIG. VELOCITY VECTORS (—— : 1.0 (M/S))

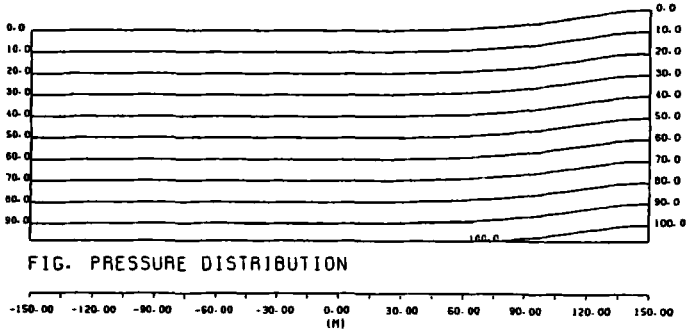

FIG. PRESSURE DISTRIBUTION

The run-up height on a right wall becomes maximum

step = 2984 , time = 29.84 (sec)

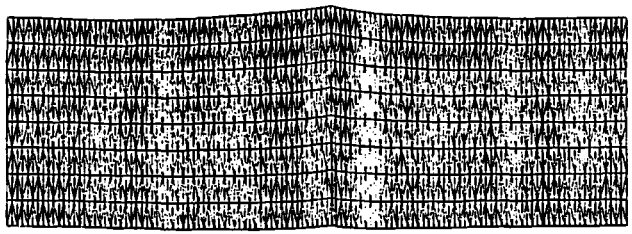

FIG. MESH DIVISION

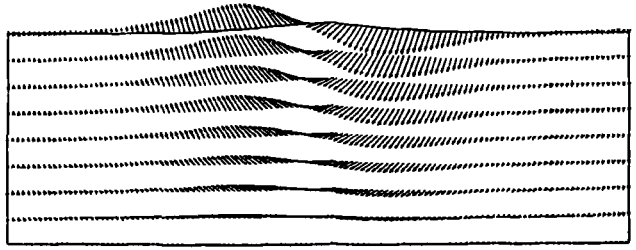

FIG. VELOCITY VECTORS (—— : 1.0 (M/S))

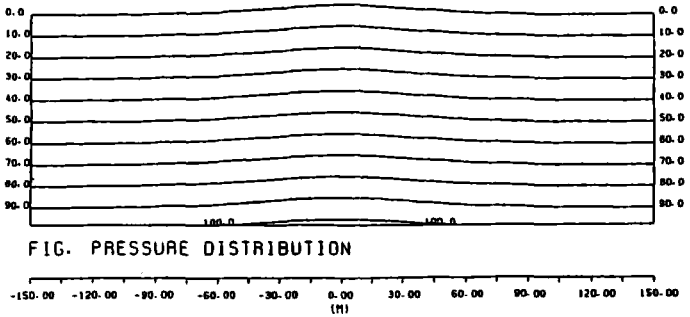

FIG. PRESSURE DISTRIBUTION

The wave returns to the center position

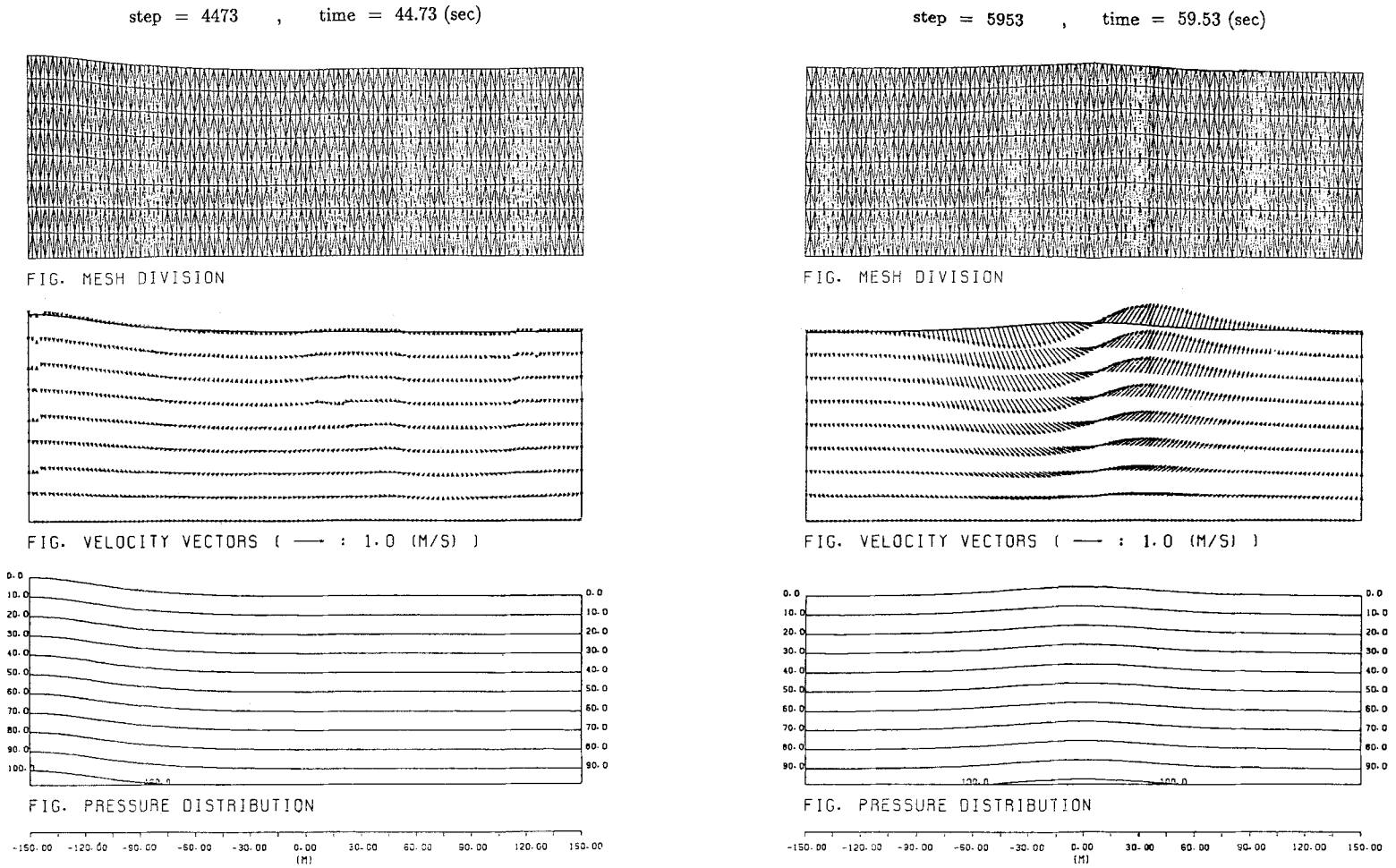

The run-up height on a left wall becomes maximum

The wave returns to the center position

Figure 8. Computed result by Method B

7. METHOD C

7.1. Basic concept

The numerical analysis referred to as Method C is described in this section. The previous two methods employed the intermediate velocity to derive the pressure Poisson equation. In contrast, Method C derives the pressure equation directly from the equation of motion. Moreover, the free surface condition of Method B is not sufficiently clear. To overcome the free surface condition, the equations of Method C are derived from the equations of motion and continuity in a direct manner. The pressure Poisson equation is derived from the following process.

Taking the divergence on both sides of equation (27), the following equation can be obtained:

$$\frac{U_{i,i}^{n+1}-U_{i,i}^{n}}{\Delta t}=-\frac{1}{\rho}P_{,ii}^{n+1}+\nu(U_{i,j}^{n}+U_{j,i}^{n})_{,ij}+F_{i,i}^{n}. \tag{110}$$

Substituting equation (28) into equation (110) leads to

$$-\frac{U_{i,i}^{n}}{\Delta t}=-\frac{1}{\rho}P_{,ii}^{n+1}+\nu(U_{i,j}^{n}+U_{j,i}^{n})_{,ij}+F_{i,i}^{n}. \tag{111}$$

Rearranging the terms, the pressure Poisson equation can be obtained:

$$P_{,ii}^{n+1}=\frac{\rho}{\Delta t}U_{i,i}^{n}+\mu(U_{i,j}^{n}+U_{j,i}^{n})_{,ij}+\rho F_{i,i}^{n}. \tag{112}$$

Referring to equation (27), velocity U_i^{n+1} is derived as follows:

$$U_i^{n+1}=U_i^{n}-\Delta t\left(\frac{1}{\rho}P_{,i}^{n+1}-\nu(U_{i,j}^{n}+U_{j,i}^{n})_{,j}-F_i^{n}\right). \tag{113}$$

The algorithm of Method C can be summarized as follows.

1. Pressure P^{n+1} is calculated:

$$P_{,ii}^{n+1}=\frac{\rho}{\Delta t}U_{i,i}^{n}+\mu(U_{i,j}^{n}+U_{j,i}^{n})_{,ij}+\rho F_{i,i}^{n}. \tag{114}$$

2. Velocity U_i^{n+1} is calculated:

$$U_i^{n+1}=U_i^{n}-\Delta t\left(\frac{1}{\rho}P_{,i}^{n+1}-\nu(U_{i,j}^{n}+U_{j,i}^{n})_{,j}-F_i^{n}\right). \tag{115}$$

3. U_i^{n+1} is replaced with U_i^{n} and proceed to the next iteration cycle.

7.2. Variational equations

To obtain the finite element equations, the variational forms should be derived. Equation (114) is multiplied by the weighting function P^* and integrated by parts over the domain V to give

$$\int_V (P_{,i}^{*}P_{,i}^{n+1})\mathrm{d}V=-\frac{\rho}{\Delta t}(P^{*}U_{i,i}^{n})\mathrm{d}V+\mu\int_V P_{,i}^{*}(U_{i,j}^{n}+U_{j,i}^{n})_{,j}\,\mathrm{d}V+\rho\int_V (P_{,i}^{*}F_i^{n})\mathrm{d}V+\Omega_i^{n+1}, \tag{116}$$

$$\Omega_i^{n+1}=\int_S (P^{*}P_{,i}^{n+1})\cdot N_i\,\mathrm{d}S-\mu\int_S P^{*}(U_{i,j}^{n}+U_{j,i}^{n})_{,j}\cdot N_i\,\mathrm{d}S-\rho\int_S (P^{*}F_i^{n})\cdot N_i\,\mathrm{d}S. \tag{117}$$

The pressure gradient $P_{,i}^{n+1}\cdot N_i$ is expressed by the following equation where the Navier–Stokes

equation is multiplied by the direction cosines of the outward normal on the boundary:

$$P_{,i}^{n+1}\cdot N_i=-\left(\rho\frac{U_i^{n+1}-U_i^n}{\Delta t}-\mu(U_{i,j}^n+U_{j,i}^n)_{,j}-\rho F_i^n\right)\cdot N_i. \tag{118}$$

Substituting equation (118) into equation (117) leads to

$$\Omega_i^{n+1}=-\int_S P^*\left(\rho\frac{U_i^{n+1}-U_i^n}{\Delta t}-\mu(U_{i,j}^n+U_{j,i}^n)_{,j}-\rho F_i^n\right)\cdot N_i\,\mathrm{d}S$$
$$-\mu\int_S P^*\,(U_{i,j}^n+U_{j,i}^n)_{,j}\cdot N_i\,\mathrm{d}S-\rho\int_S (P^*F_i^n)\cdot N_i\,\mathrm{d}S. \tag{119}$$

Only the first term of equation (119) remains and it is obtained that

$$\Omega_i^{n+1}=-\rho\int_S P^*\left(\frac{U_i^{n+1}-U_i^n}{\Delta t}\right)\cdot N_i\,\mathrm{d}S. \tag{120}$$

Using a linear interpolation function, the second term of the right-hand side of equation (116) is dropped:

$$\int_V (P_{,i}^* P_{,i}^{n+1})=-\frac{\rho}{\Delta t}\int_V (P^*U_{i,i}^n)\mathrm{d}V+\rho\int_V (P_{,i}^*F_i^n)\mathrm{d}V+\Omega_i^{n+1}. \tag{121}$$

Equation (115) is multiplied by the weighting function U_i^* and integrated by parts over the domain V to give

$$\int_V (U_i^*U_i^{n+1})\mathrm{d}V=\int_V (U_i^*U_i^n)\mathrm{d}V+\Delta t\left(\frac{1}{\rho}\int_V (U_{i,i}^*P^{n+1})\mathrm{d}V-\nu\int_V U_{i,j}^*(U_{i,j}^n+U_{j,i}^n)\mathrm{d}V\right.$$
$$\left.+\int_V (U_i^*F_i^n)\mathrm{d}V+\Sigma_i^n\right), \tag{122}$$

$$\Sigma_i^n=\int_S U_i^*\left(-\frac{1}{\rho}P^{n+1}\cdot\delta_{ij}+\nu(U_{i,j}^n+U_{j,i}^n)\right)\cdot N_j\,\mathrm{d}S. \tag{123}$$

7.3. *Boundary conditions*

The boundary conditions in Figure 9 can be explained as follows:

(i)
$$\Omega_i^{n+1}=-\rho\int_S P^*\left(\frac{U_i^{n+1}-U_i^n}{\Delta t}\right)\cdot N_i\,\mathrm{d}S=\hat{r}_i \qquad \text{on } S_1, \tag{124}$$

$$P^{n+1}=\hat{P} \qquad \text{on } S_2; \tag{125}$$

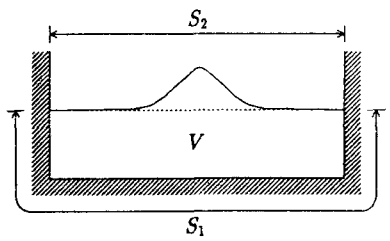

Figure 9. Boundary condition

(ii) $$U_i^{n+1} = \hat{U}_i \quad \text{on } S_1, \tag{126}$$

$$\left(-\frac{1}{\rho}P^{n+1}\cdot\delta_{ij} + \nu(U^n_{i,j}+U^n_{j,i})\right)\cdot N_j = \hat{t}_i = 0 \quad \text{on } S_2. \tag{127}$$

Item (i) is the boundary condition for the pressure Poisson equation (114). Referring to equation (124), the velocity at the $(n+1)$th time point, U_i^{n+1}, is required to compute the term Ω_i^{n+1}. Generally, U_i^{n+1} is an unknown variable. However, in the computation of the rectangular channel shown in Figure 9 the term Ω_i^{n+1} can be computed as zero, because the product $U_i^{n+1}\cdot N_i$ is always zero. Item (ii) is the boundary condition for equation (115).

7.4. *Finite element equations*

The finite element equations can be derived in the following form from equations (121) and (122) using the interpolation function equations (31) and (32) and the weighting function equations (33) and (34):

$$A^{n+1}_{\alpha i\beta i}P^{n+1}_\beta = -\frac{\rho}{\Delta t}H^n_{\alpha\beta i}U^n_{\beta i} + \rho N^n_{\alpha i}F^n_{\alpha i} + \hat{\Omega}^{n+1}_i, \tag{128}$$

$$\bar{M}^{n+1}_{\alpha\beta}U^{n+1}_{\beta i} = \bar{M}^n_{\alpha\beta}U^n_{\beta i} + \Delta t\left(\frac{1}{\rho}H^{n+1}_{\alpha i\beta}P^{n+1}_\beta - \nu S^n_{\alpha i\beta j}U^n_{\beta j} + N^n_\alpha F^n_{\alpha i} + \hat{\Sigma}^n_{\alpha i}\right), \tag{129}$$

where

$$M_{\alpha\beta} = \int_V (\Phi_\alpha\Phi_\beta)\mathrm{d}V, \qquad N_\alpha = \int_V (\Phi_\alpha)\mathrm{d}V, \qquad N_{\alpha i} = \int_V (\Phi_{\alpha,i})\mathrm{d}V,$$

$$S_{\alpha i\beta j} = \int_V (\Phi_{\alpha,k}\Phi_{\beta,k})\mathrm{d}V\cdot\delta_{ij} + \int_V (\Phi_{\alpha,j}\Phi_{\beta,i})\mathrm{d}V,$$

$$A_{\alpha i\beta i} = \int_V (\Phi_{\alpha,i}\Phi_{\beta,i})\mathrm{d}V, \quad H_{\alpha\beta i} = \int_V (\Phi_\alpha\Phi_{\beta,i})\mathrm{d}V, \quad H_{\alpha i\beta} = H^{\mathrm{T}}_{\alpha\beta i},$$

$$\hat{\Omega}_{\alpha i} = \int_S (\Phi_\alpha \hat{r}_i)\mathrm{d}S, \qquad \hat{\Sigma}_{\alpha i} = \int_S (\Phi_\alpha \hat{t}_i)\mathrm{d}S,$$

in which $\bar{M}_{\alpha\beta}$ means the lumped mass matrix obtained from the consistent matrix $M_{\alpha\beta}$.

7.5. *Algorithm*

The algorithm of the Lagrangian finite element method using Method C can be expressed in the following forms:

(a) Set $m=0$ and $U_i^{n+1(0)}$ is assigned as U_i^n.
(b) The co-ordinates of the nodal points $X_i^{n+1(m)}$ are calculated:

$$X_i^{n+1(m)} = X_i^n + \frac{\Delta t}{2}(U_i^{n+1(m)} + U_i^n). \tag{130}$$

(c) Pressure $P^{n+1(m+1)}$ is calculated:

$$A^{n+1}_{\alpha i\beta i}P^{n+1(m+1)}_\beta = -\frac{\rho}{\Delta t}H^n_{\alpha\beta i}U^n_{\beta i} + \rho N^n_{\alpha i}F^n_{\alpha i} + \hat{\Omega}^{n+1}_i. \tag{131}$$

(d) Velocity $U_i^{n+1(m+1)}$ is calculated:

$$\bar{M}_{\alpha\beta}^{n+1} U_{\beta i}^{n+1(m+1)} = \bar{M}_{\alpha\beta}^{n} U_{\beta i}^{n} + \Delta t\left(\frac{1}{\rho} H_{\alpha i\beta}^{n+1} P_{\beta}^{n+1(m+1)} - \nu S_{\alpha i\beta j}^{n} U_{\beta j}^{n} + N_{\alpha}^{n} F_{\alpha i}^{n} + \hat{\Sigma}_{\alpha i}^{n}\right). \tag{132}$$

(e) If $|U_i^{n+1(m+1)} - U_i^{n+1(m)}| < \varepsilon$ is not satisfied, then $m = m+1$ and return to step (b).
(f) $U_i^{n+1(m+1)}$ is replaced with U_i^n and proceed to the next iteration cycle.

The number of iterations within one time point is denoted by (m).

7.6. *Numerical study*

Figure 10 shows the finite element mesh representing the solitary wave propagation, the computed velocity and pressure at the times when the run-up height of a solitary wave on a right wall becomes maximum, when the wave returns to the centred position, when the run-up height of a solitary wave on a left wall becomes maximum and when the wave returns to the centred position again. The final computed results should be coincident with the initial configuration because the viscosity is neglected in this computation. Identical results have been obtained, which shows that the algorithm of Method C is adaptable to the analysis of free surface flows such as solitary wave propagation.

8. METHOD D

8.1. *Basic concept*

The numerical analysis referred to as Method D is described in this section. To compute the term Ω_i^{n+1} on the left-hand side of equation (120), it is necessary to know the velocity at the $(n+1)$th time point. At the time of computing P^{n+1}, velocity U_i^{n+1} is not yet known. Therefore iteration is required. The formulation of Method D is the same as that of Method C except for the introduction of iteration. The basic concept can be written as follows.

1 Set $m=0$ and pressure $P^{n+1(m)}$ is calculated:

$$P_{,ii}^{n+1(m)} = \frac{\rho}{\Delta t} U_{i,i}^{n} + \mu(U_{i,j}^{n} + U_{j,i}^{n})_{,ij} + \rho F_{i,i}^{n}. \tag{133}$$

2. Velocity $U_i^{n+1(m)}$ is calculated:

$$U_i^{n+1(m)} = U_i^{n} - \Delta t\left(\frac{1}{\rho} P_{,i}^{n+1(m)} - \nu(U_{i,j}^{n} + U_{j,i}^{n})_{,j} - F_i^{n}\right). \tag{134}$$

3. Pressure $P^{n+1(m+1)}$ is calculated:

$$P_{,ii}^{n+1(m+1)} = \frac{\rho}{\Delta t} U_{i,i}^{n} + \mu(U_{i,j}^{n+1(m)} + U_{j,i}^{n+1(m)})_{,ij} + \rho F_{i,i}^{n+1}. \tag{135}$$

4 Velocity $U_i^{n+1(m+1)}$ is calculated:

$$U_i^{n+1(m+1)} = U_i^{n} - \Delta t\left(\frac{1}{\rho} P_{,i}^{n+1(m+1)} - \nu(U_{i,j}^{n+1(m)} + U_{j,i}^{n+1(m)})_{,j} - F_i^{n+1}\right). \tag{136}$$

5. If $|U_i^{n+1(m+1)} - U_i^{n+1(m)}| < \varepsilon$ is not satisfied, then $m = m+1$ and return to step 3.
6. $U_i^{n+1(m+1)}$ is replaced with U_i^n and proceed to the next iteration cycle.

step = 1491 , time = 14.91 (sec)

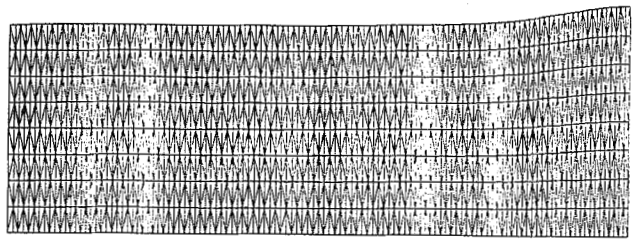

FIG. MESH DIVISION

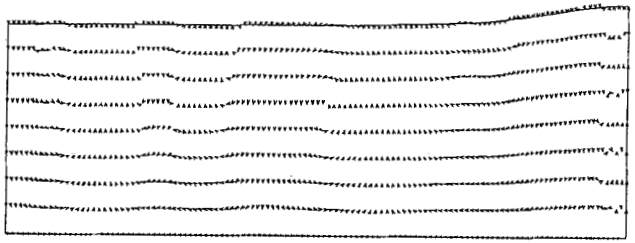

FIG. VELOCITY VECTORS (—— : 1.0 (M/S))

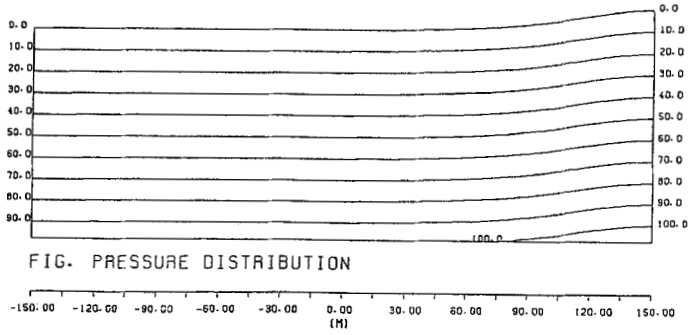

FIG. PRESSURE DISTRIBUTION

The run-up height on a right wall becomes maximum

step = 2984 , time = 29.84 (sec)

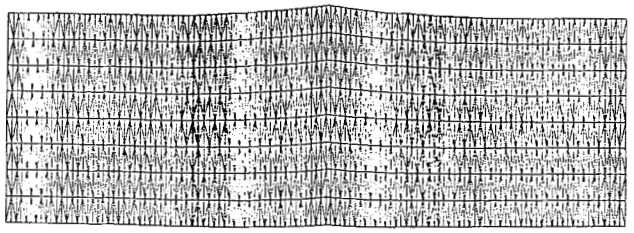

FIG. MESH DIVISION

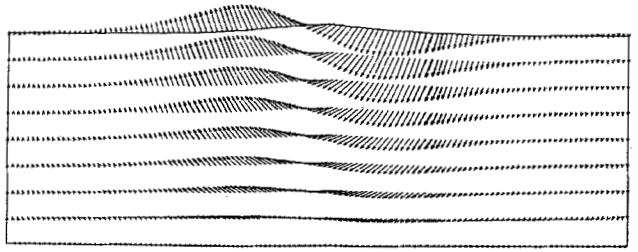

FIG. VELOCITY VECTORS (—— : 1.0 (M/S))

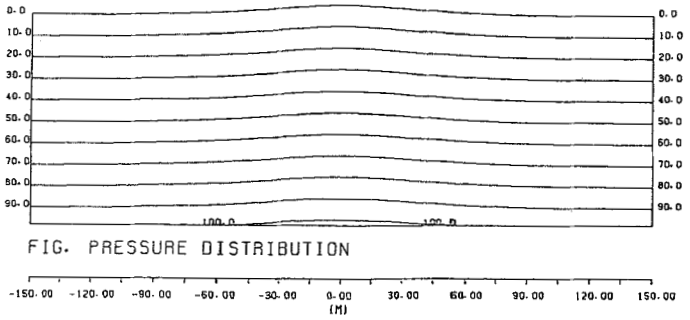

FIG. PRESSURE DISTRIBUTION

The wave returns to the center position

step = 4473 , time = 44.73 (sec)

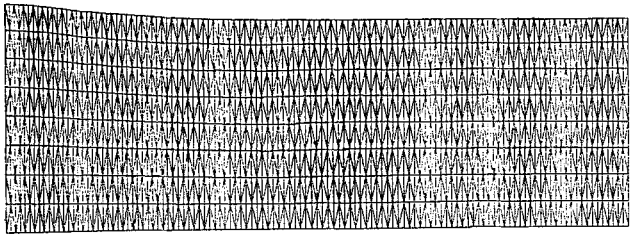

FIG. MESH DIVISION

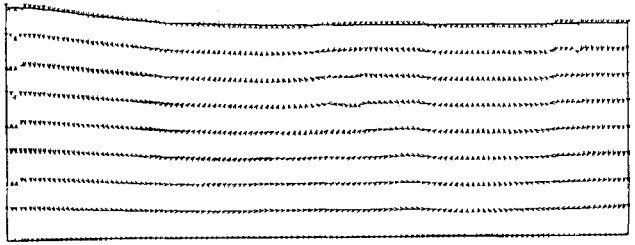

FIG. VELOCITY VECTORS (—— : 1.0 (M/S))

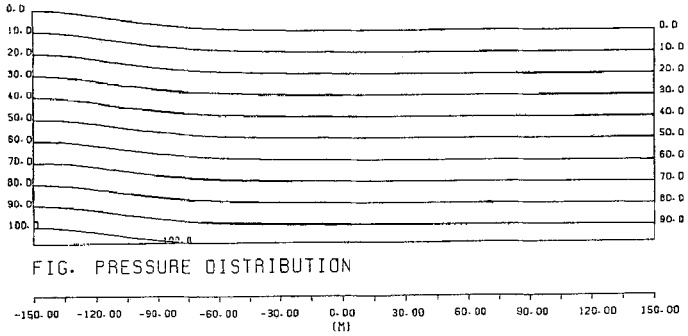

FIG. PRESSURE DISTRIBUTION

The run-up height on a left wall becomes maximum

step = 5953 , time = 59.53 (sec)

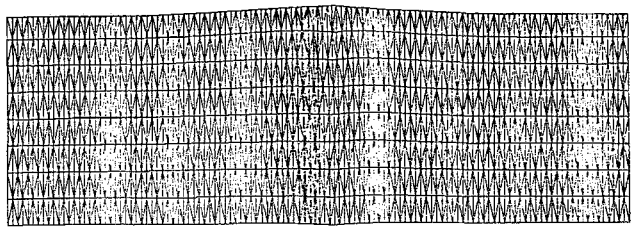

FIG. MESH DIVISION

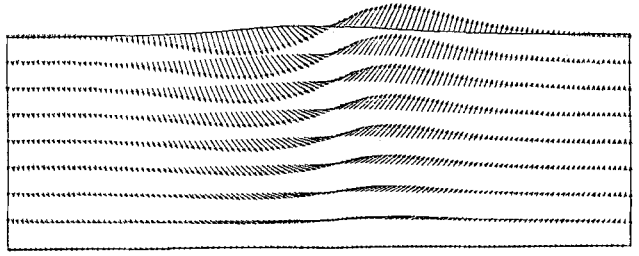

FIG. VELOCITY VECTORS (—— : 1.0 (M/S))

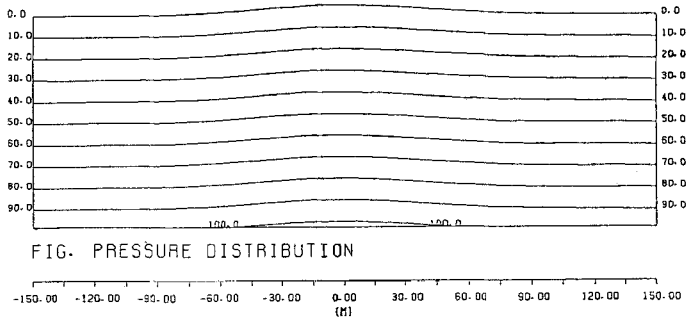

FIG. PRESSURE DISTRIBUTION

The wave returns to the center position

Figure 10. Computed result by Method C

8.2. Boundary conditions

The boundary conditions in Figure 11 can be explained as follows:

(i)
$$\Omega_i^{n+1} = -\rho \int_S P^* \left(\frac{U_i^{n+1} - U_i^n}{\Delta t} \right) \cdot N_i \, dS = \hat{r}_i \qquad \text{on } S_1, \tag{137}$$

$$P^{n+1} = \hat{P} \qquad \text{on } S_2; \tag{138}$$

(ii)
$$U_i^{n+1} = \hat{U}_i \qquad \text{on } S_1, \tag{139}$$

$$\left(-\frac{1}{\rho} P^{n+1} \cdot \delta_{ij} + \nu (U_{i,j}^{n+1} + U_{j,i}^{n+1}) \right) \cdot N_j = \hat{t}_i = 0 \qquad \text{on } S_2. \tag{140}$$

Item (i) is the boundary condition for the pressure Poisson equation. Item (ii) is the boundary condition for equation (136). This free surface boundary condition must be evaluated at the $(n+1)$th time step essentially. Using the iterative method, this objective can be attained.

8.3. Algorithm

The algorithm of the Lagrangian finite element method using Method D can be expressed using the notations given in equations (128) and (129).

(a) Set $m=0$ and $U_i^{n+1(0)}$ is assigned as U_i^n.

(b) The co-ordinates of the nodal points $X_i^{n+1(m)}$ are calculated:

$$X_i^{n+1(m)} = X_i^n + \frac{\Delta t}{2} (U_i^{n+1(m)} + U_i^n). \tag{141}$$

(c) Pressure $P^{n+1(m)}$ is calculated:

$$A_{\alpha i \beta i}^{n+1} P_\beta^{n+1(m)} = -\frac{\rho}{\Delta t} H_{\alpha \beta i}^n U_{\beta i}^n + \rho N_{\alpha i}^n F_{\alpha i}^n. \tag{142}$$

(d) Velocity $U_i^{n+1(m)}$ is calculated:

$$\bar{M}_{\alpha\beta}^{n+1} U_{\beta i}^{n+1(m)} = \bar{M}_{\alpha\beta}^n U_{\beta i}^n + \Delta t \left(\frac{1}{\rho} H_{\alpha i \beta}^{n+1} P_\beta^{n+1(m)} - \nu S_{\alpha i \beta j}^n U_{\beta j}^n + N_\alpha^n F_{\alpha i}^n + \hat{\Sigma}_{\alpha i}^n \right). \tag{143}$$

(e) The co-ordinates of the nodal points $X_i^{n+1(m+1)}$ are calculated:

$$X_i^{n+1(m+1)} = X_i^n + \frac{\Delta t}{2} (U_i^{n+1(m)} + U_i^n). \tag{144}$$

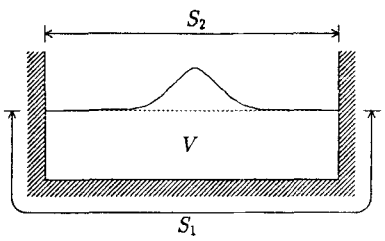

Figure 11. Boundary condition

(f) Pressure $P^{n+1(m+1)}$ is calculated:

$$A^{n+1}_{\alpha i\beta i} P^{n+1(m+1)}_{\beta} = -\frac{\rho}{\Delta t} H^{n}_{\alpha\beta i} U^{n}_{\beta i} + \rho N^{n+1}_{\alpha i} F^{n+1}_{\alpha i} + \hat{\Omega}^{n+1}_{i} . \tag{145}$$

(g) Velocity $U_i^{n+1(m+1)}$ is calculated:

$$\bar{M}^{n+1}_{\alpha\beta} U^{n+1(m+1)}_{\beta i} = \bar{M}^{n}_{\alpha\beta} U^{n}_{\beta i} + \Delta t\left(\frac{1}{\rho} H^{n+1}_{\alpha i\beta} P^{n+1(m+1)}_{\beta} - \nu S^{n+1}_{\alpha i\beta j} U^{n+1(m)}_{\beta j} + N^{n+1}_{\alpha} F^{n+1}_{\alpha i} + \hat{\Sigma}^{n+1}_{\alpha i}\right). \tag{146}$$

(h) If $|U_i^{n+1(m+1)} - U_i^{n+1(m)}| < \varepsilon$ is not satisfied, then $m = m+1$ and return to step (e).
(i) $U_i^{n+1(m+1)}$ is replaced with U_i^n and proceed to the next iteration cycle.

The number of iterations within one time point is denoted by (m).

8.4. Numerical study

Figure 12 shows the finite element mesh representing the solitary wave propagation, the computed velocity and pressure at the times when the run-up height of a solitary wave on a right wall becomes maximum, when the wave returns to the centred position, when the run-up height of a solitary wave on a left wall becomes maximum and when the wave returns to the centred position again. The final computed results should be coincident with the initial configuration because the viscosity is neglected in this computation. Identical results have been obtained, which shows that the algorithm of Method D is adaptable to the analysis of free surface flows such as solitary wave propagation.

9. COMPARISON OF METHODS OF SOLUTION

The run-up height is calculated and compared with the analytical solution. The arrival time at which the wave will have the maximum value is calculated by equations (37) and (42). The wave height is computed by equation (40) and the computed error is evaluated as

$$E = \frac{|R - R_C|}{R} \times 100\% , \tag{147}$$

where R is the analytical solution and R_C is the calculated run-up height. Tables IV–VII show the comparison of the wave height and the arrival time at the times when the wave runs up on the right wall, when the wave returns to the centre position, when the wave runs up on the left wall and when the wave returns to the centre position. The ratio of the computed value to the analytical value is also represented. All values show good agreement. The ratio of wave height to water depth for Example 1 is rather small. The deformation of the wave is moderate. Therefore the distortion of the mesh is insignificant. The analysis can be continued without the rezoning technique.

10. DISCUSSION

As stated in Section 3, the purpose of the present paper is to investigate the solution method of unknown variables U_i^{n+1} and P^{n+1} satisfying the differential equations (27) and (28) with boundary condition equations (29) and (30) starting from the known variables U^n and P^n. To obtain a stable computation, the fractional step method employs the fact that the equation of

step = 1491 , time = 14.91 (sec)

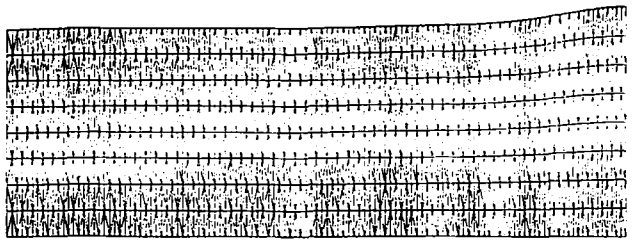

FIG. MESH DIVISION

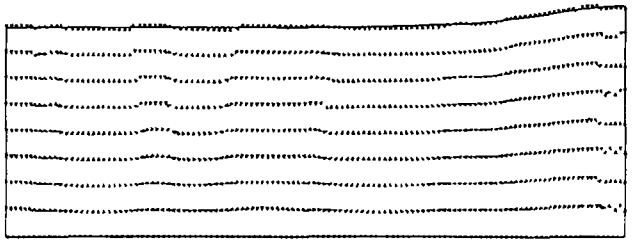

FIG. VELOCITY VECTORS (—— : 1.0 (M/S))

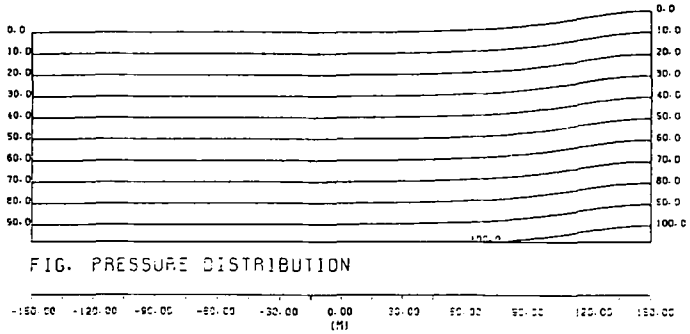

FIG. PRESSURE DISTRIBUTION

The run-up height on a right wall becomes maximum

step = 2984 , time = 29.84 (sec)

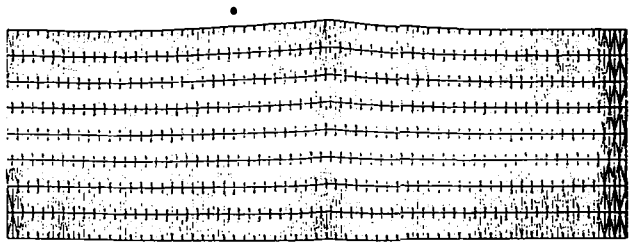

FIG. MESH DIVISION

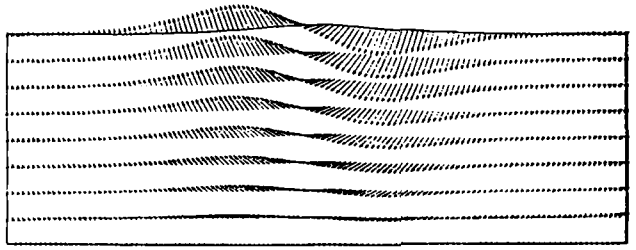

FIG. VELOCITY VECTORS (—— : 1.0 (M/S))

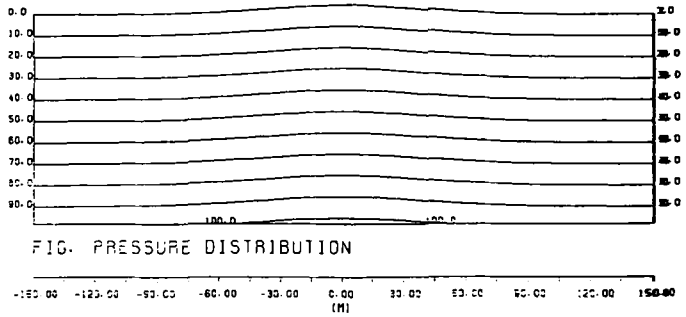

FIG. PRESSURE DISTRIBUTION

The wave returns to the center position

step = 4472 , time = 44.72 (sec)

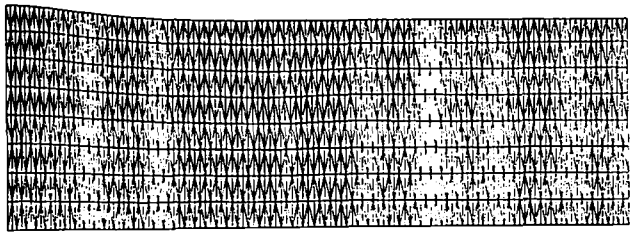

FIG. MESH DIVISION

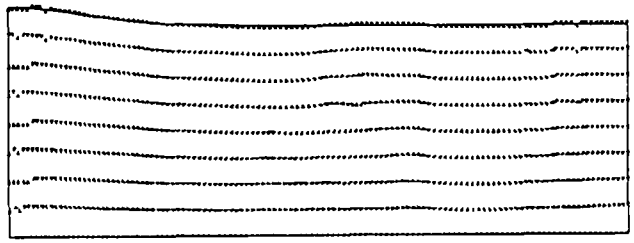

FIG. VELOCITY VECTORS (—— : 1.0 (M/S))

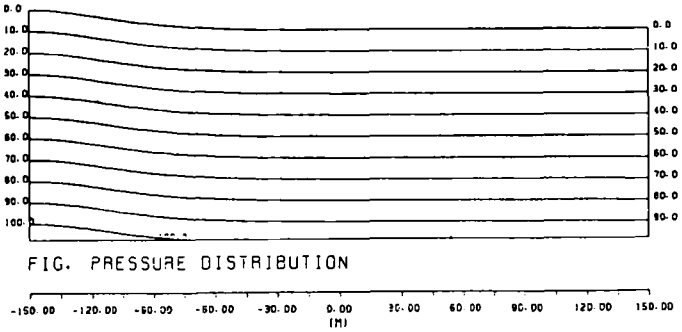

FIG. PRESSURE DISTRIBUTION

The run-up height on a left wall becomes maximum

step = 5953 , time = 59.53 (sec)

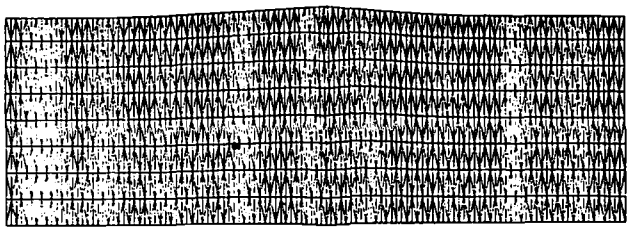

FIG. MESH DIVISION

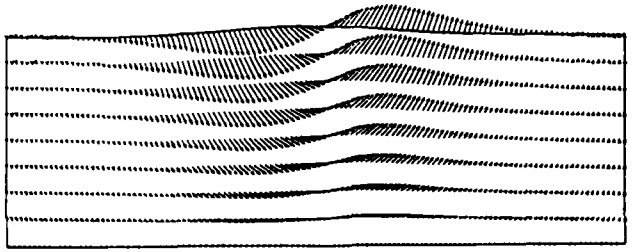

FIG. VELOCITY VECTORS (—— : 1.0 (M/S))

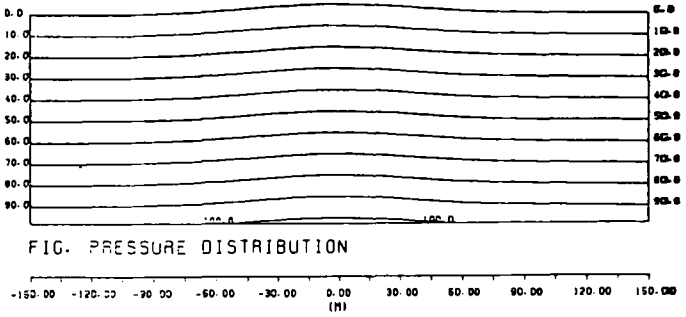

FIG. PRESSURE DISTRIBUTION

The wave returns to the center position

Figure 12. Computed result by Method D

Table IV. Comparison at the time when the wave runs up on the right wall

Method	Wave height (m)	Arrival time (s)	E (%)
A	1·0264	14·91	1·37
B	1·0263	14·91	1·36
C	1·0261	14·91	1·34
D	1·0261	14·91	1·34
Analytical	1·0125	14·79	—

Table V. Comparison at the time when the wave returns to the centre position

Method	Wave height (m)	Arrival time (s)	E (%)
A	0·5022	29·82	0·44
B	0·5014	29·84	0·28
C	0·5013	29·84	0·26
D	0·5014	29·84	0·28
Analytical	0·5000	29·57	—

Table VI. Comparison at the time when the wave runs up on the left wall

Method	Wave height (m)	Arrival time (s)	E (%)
A	1·0262	44·73	1·35
B	1·0244	44·73	1·18
C	1·0240	44·73	1·14
D	1·0237	44·72	1·11
Analytical	1·0125	44·36	—

Table VII. Comparison at the time when the wave returns to the centre position

Method	Wave height (m)	Arrival time (s)	E (%)
A	0·5026	59·52	0·52
B	0·5012	59·53	0·24
C	0·5008	59·53	0·16
D	0·5009	59·53	0·18
Analytical	0·5000	59·15	—

motion is differentiated with respect to co-ordinates to consider the equation of continuity. Thus, to correlate the resultant equations with the original equations, new boundary conditions must be introduced.

In Method A pressure is computed from equation (50), which is derived from equation (49) with the integral constant considered zero. Multiplying equation (49) by unit normal N_i and using the equation

$$\phi_{,i} \cdot N_i = \hat{r} = 0 \quad \text{on } S_1 \tag{148}$$

leads to the following form:

$$P_{,i}^{n+1} \cdot N_i = P_{,i}^{n} \cdot N_i \quad \text{on } S_1 . \tag{149}$$

This means that the normal gradient of pressure on the boundary S_1, $\partial P/\partial N_i$, at the $(n+1)$th time point should be coincident with $\partial P/\partial N_i$ at the nth time point on the boundary S_1. Thus it is seen that Method A is only valid if equation (149) is always valid on the boundary S_1. Considering the solitary wave problem, equation (149) is valid.

In Method B the boundary condition for pressure is not very clear. In the authors' numerical computations, equations (94) and (95) were used. The computed results were in good agreement with the analytical solution. However, this condition can be used only for the solitary wave propagation problem and is not adaptable to the more general problem. Moreover, Method B employs equations (86) and (88) as the boundary condition for the equation of motion on the free surface boundary. These equations are not exact in describing the boundary condition equation (6) on the free surface. Thus Method B is not always suitable for general numerical computation in spite of the fact that the computation is stable.

In Method C the boundary condition for the free surface is

$$\left(-\frac{1}{\rho}P^{n+1}\cdot\delta_{ij}+\nu(U^n_{i,j}+U^n_{j,i})\right)\cdot N_j=\hat{t}_i=0 \quad \text{on } S_2; \tag{150}$$

but precisely, this condition should be

$$\left(-\frac{1}{\rho}P^{n+1}\cdot\delta_{ij}+\nu(U^{n+1}_{i,j}+U^{n+1}_{j,i})\right)\cdot N_j=\hat{t}_i=0 \quad \text{on } S_2. \tag{151}$$

To introduce the boundary condition equation (151), the iteration method must be introduced. This is the reason why Method D is employed. From the authors' numerical computations, there is no difference between the results by Method C and those by Method D. Therefore it is concluded that Method C is the most recommendable for fluid flow analysis by the fractional step method.

To pursue the limitation of the present Lagrangian method, Example 2 is analysed employing Method C. The dimensions and conditions of the solitary wave in Example 2 are represented in Tables II and III. Figure 13 shows the computed result at the time when the run-up height of a solitary wave on a right wall becomes maximum. A comparison for Example 2 is given in Table VIII. The computed wave height at the time when the wave runs up on the right wall and the arrival time are represented. The computations were terminated because of the extreme distortion of the finite element mesh. Looking at Figure 14, unexpected velocity distributions are computed. The computation was tried using a shorter time increment but there was no improvement. Thus in cases where the ratio of the wave height to the water depth, α, is large, the rezoning technique should be introduced. In example 1 we used $\alpha=0{\cdot}05$ and in Example 2, $\alpha=0{\cdot}2$. Therefore computation by the Lagrangian description could be useful with α less than 0·2 for solitary wave propagation.

11. CONCLUSIONS

The results of this paper can be summarized as follows.

1. A finite element method based on the Lagrangian description has been presented to solve unsteady viscous fluid flow with a moving free surface. The Lagrangian method is suitable to pursue the free surface position because the nodal points of the flow field always move with the fluid.
2. To solve the finite element equation, the fractional step method has been used. The advantage of this method is to be able to use the same interpolation function for both velocity and pressure. This simplifies the computation.

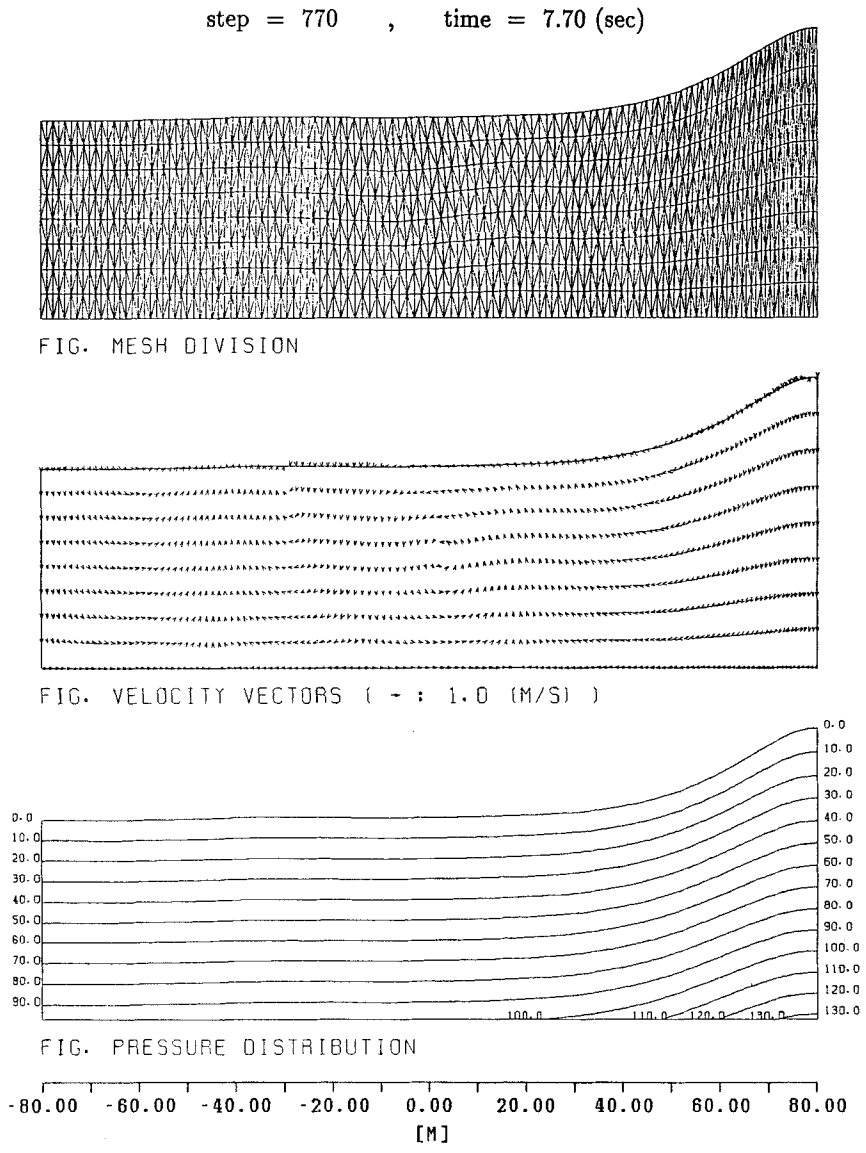

Figure 13. Computed result when the run-up height on a right wall becomes maximum by Method C

Table VIII. Comparison at the time when the wave runs up on the right wall

Method	Wave height (m)	Arrival time (s)	E (%)
C	4·4859	7·70	6·81
Analytical	4·2000	7·38	—

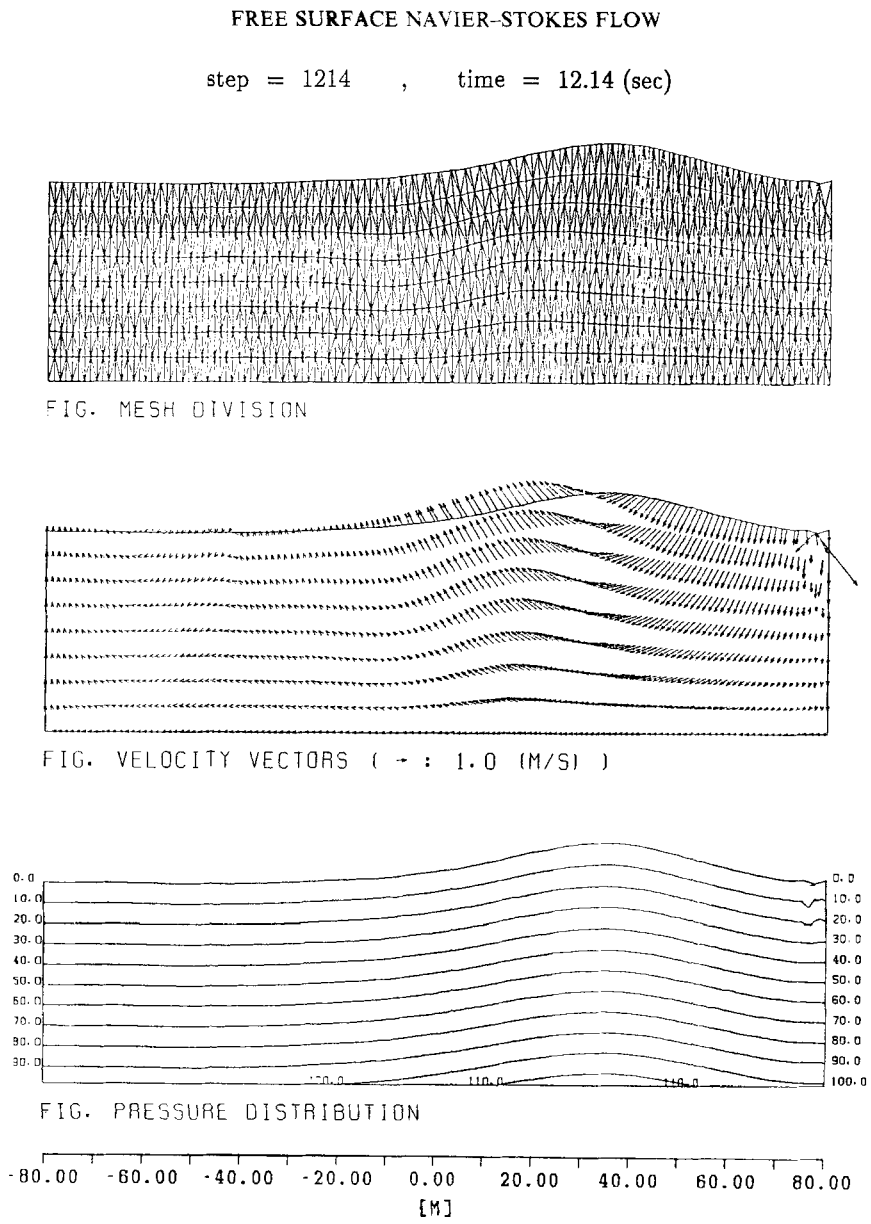

Figure 14. The calculation is divergent

3. Four variations of the fractional step method are presented and compared with each other. It is concluded that Method C is recommendable for practical computations.
4. The fractional step methods previously presented by the authors' group are effective, but attention must be paid to how to impose the boundary condition, especially for the condition of pressure.
5. To solve solitary wave propagation with moderate wave height, the Lagrangian method is suitable, but to solve the high-wave propagation problem, an improvement such as the arbitrary Lagrangian–Eulerian method must be introduced.

ACKNOWLEDGEMENTS

The computation has been carried out using the FACOM VP-30 computer of Chuo University. A part of this research was supported by Grant in Aid of Science and Engineering, Ministry of Education, No. 01613001.

REFERENCES

1. A. J. Chorin, 'Numerical solution of the Navier–Stokes equations', *Math. Comput.*, **22,** 745–762 (1968).
2. J. Dona, S. Giuliani, H. Laval and L. Quartapelle, 'Solution of the unsteady Navier–Stokes equations by a finite element projection method', in C. Taylor and K. Morgan (eds), *Computational Techniques in Transient and Turbulent Flow*, Pineridge, Swansea, 1981, pp. 97–132.
3. J. Donea, S. Giuliani and H. Laval, 'Finite element solution of the unsteady Navier–Stokes equations by a fractional step method', *Comput. Methods Appl. Mech. Eng.*, **32,** 53–73 (1982).
4. G. E. Schneider, G. D. Raithby and M. M. Yovanovich, 'Finite element solution procedures for solving the incompressible, Navier–Stokes equations using equal order variable interpolation', *Numer. Heat Transfer*, **1,** 435–451 (1978).
5. G. E. Schneider and G. D. Raithby, 'Finite element analysis of incompressible fluid flow incorporating equal order pressure and velocity interpolation', in K. Morgan *et al.* (eds), *Computer Methods in Fluids*, Pentech, London, 1980, pp. 49–83.
6. R. Glowinsky, B. Mantel, J. Periaux, P. Perrier and O. Pirronneau, 'On an efficient new preconditioned conjugate gradient method. Application to the in-core solution of the Navier–Stokes equations via non-linear least-square and finite element method', in R. H. Gallagher et al. (eds), *Finite Elements in Fluids, Vol. 4*, Wiley, Chichester, 1982, pp. 365–401.
7. A. Mizukami and M. Tsuchiya, 'A finite element method for the three dimensional non-linear Navier–Stokes equations', *Int. j. numer. methods fluids*, **4,** 349–357 (1984).
8. M. Kawahara and K. Ohmiya, 'Finite element analysis of density flow using the velocity correction method', *Int. j. numer. methods fluids*, **5,** 981–993 (1985).
9. B. Ramaswamy, M. Kawahara and T. Nakayama, 'Lagrangian finite element method for the analysis of two-dimensional sloshing problems', *Int. j. numer. methods fluids*, **6,** 659–670 (1986).
10. B. Ramaswamy and M. Kawahara, 'Lagrangian finite element analysis applied to viscous free surface fluid flow', *Int. j. numer. methods fluids*, **7,** 953–984 (1987).
11. M. Kawahara and A. Anjyu, 'Lagrangian finite element method for solitary wave propagation', *Comput. Methods*, **2,** 299–307 (1988).
12. B. Ramaswamy and M. Kawahara, 'Arbitrary Lagrangian–Eulerian finite element method for unsteady, convective, incompressible viscous free surface fluid flow', *Int. j. numer. methods fluids*, **7,** 1053–1075 (1987).
13. E. V. Laitone, 'The second approximation to cnoidal and solitary waves', *J. Fluid. Mech.*, **9,** 430–444 (1960).